geosciences

MDPI

*Article*

# The Coastal Areas of the Bay of Naples: The Sedimentary Dynamics and Geological Evolution of the Naples Canyons

**Gemma Aiello [1,*] and Mauro Caccavale [1,2]**

[1] Istituto di Scienze Marine (ISMAR), Consiglio Nazionale delle Ricerche (CNR), Sezione Secondaria di Napoli, 80133 Napoli, Italy; mauro.caccavale@cnr.it
[2] Istituto Nazionale di Geofisica e Vulcanologia (INGV), Osservatorio Vesuviano (OV), Via Diocleziano, 80128 Napoli, Italy
* Correspondence: gemma.aiello@cnr.it; Tel.: +39-81-8960050 or +39-81-5423820

**Abstract:** The sedimentary dynamics and geological evolution of the Naples canyons during the Late Quaternary have been studied based on sedimentological and seismo-stratigraphic data. Several factors, including the sedimentary environments, tectonic setting, and volcanic eruptions, have controlled the geological evolution of the coastal and marine areas of the Bay of Naples. The main data and methods include the sedimentological data analysis, the seismo-stratigraphic techniques applied in the geological interpretation of seismic profiles, and the integrated analysis of core data that were previously published. The formation of the Dohrn canyon is controlled by fluvial processes, active in correspondence with the palaeo-Schiazzano River system and by the main eruptive events involving the submarine portion of Naples Bay, including the Campanian Ignimbrite (CI; 39 ky B.P.) and the Neapolitan Yellow Tuff (NYT; 15 ky B.P.). The formation of the Magnaghi canyon is controlled by erosional processes on the continental slope of Procida Island, which was active during the last eruptive phases of the island (Solchiaro Formation; 18 ky B.P.), triggering high rates of volcaniclastic supply.

**Keywords:** sedimentary processes; coastal and marine areas; Bay of Naples; Naples canyons; sedimentary environments; volcanic eruptions



**Citation:** Aiello, G.; Caccavale, M. The Coastal Areas of the Bay of Naples: The Sedimentary Dynamics and Geological Evolution of the Naples Canyons. *Geosciences* **2023**, *13*, 226. https://doi.org/10.3390/geosciences13080226

Academic Editors: Angelos G. Maravelis and Jesus Martinez-Frias

Received: 31 May 2023
Revised: 24 July 2023
Accepted: 26 July 2023
Published: 27 July 2023



## 1. Introduction

Canyons and gullies are a critical link between coastal and shelf waters and abyssal depths, and they are responsible for transferring sediments, nutrients, and even litter and pollutants into deep-water settings [1–4]. The formation of the Dohrn canyon in Naples Bay is genetically related to the main eruptive events involving its submarine portion, including the Campanian Ignimbrite (CI; 37 ky B.P.) [5] and the Neapolitan Yellow Tuff (NYT; 15 ky B.P.) [6], recently correlated with the main tephra levels occurring in the Northern Phlegrean Fields offshore [7]. A high volcaniclastic supply during the volcanic eruptions involving the Neapolitan area has probably controlled the individuation of the Dohrn canyon's western branch. The development of the eastern branch, joining a palaeo-valley located offshore the Sorrento Peninsula, has been influenced by the high sedimentary input related to the Schiazzano river mouth [8].

The submarine canyons are significant erosional features of the sea bottom, cutting deeply through long belts of continental slopes and serving as a primary conduit through which both siliciclastic and volcaniclastic materials emanating from the coastal zones reach the deep oceanic basins [9–15]. Geological research on the Neogene evolution of the main continental margins of the Mediterranean, North Atlantic, and Pacific areas has confirmed the occurrence of large palaeo-channels, often interlayered in the Quaternary deposits of the sedimentary basins, suggesting that the origin of these kinds of canyons could be genetically related to the subaerial environment [16–25]. The morphology and the geologic evolution of the submarine canyons located on the main continental margins of the world,

based on their morphological parameters, have been deeply studied [18], including the depth range, the slope gradient, the trending of both the canyon and the related tectonic lineaments, the canyon's shape (depositional U-shape and erosional V-shape), and the canyon's profile (rectilinear or meandering).

The global canyon database of Harris et al. [2] is based on 9477 submarine canyons, using as input variables the length, the width, the mean canyon depth, the canyon depth range or delta depth, the canyon spacing, and the occurrence of shelf-incising canyons [3]. In the Mediterranean area, the canyon geomorphology is strongly controlled by the class 4, characterized by a small area, by a short length, by a narrow width, and by a close spacing between the canyons [1]. The geomorphologic map [2] has identified 9477 submarine canyons. Harris et al. [2] computed the mean values of the canyon area and the length for the global dataset, reporting the mean incision depths for shelf and slope canyons. The slope canyons exhibit larger depths and shorter lengths compared to canyons carving the continental shelf. The latitude influences the geomorphological setting of the submarine canyons, as highlighted by the different characteristics of the canyons located in polar and non-polar regions [1].

More recently, Buhrig et al. [14] compiled an updated database of submarine canyons focusing on the statistical analysis of the geomorphological parameters, including the maximum and average canyon dimensions, the canyon sinuosity, the average canyon thalweg gradient, and the maximum canyon sidewall steepness [14]. The scaling relationships between canyon morphometric parameters and correlations with the attributes of the canyon physiographic settings, terrestrial catchments, and continental shelves and slopes have been quantitatively assessed. The oceanographic processes, including the upwelling and the alongshore and the alongslope currents also influence the canyon morphology.

The source-to-sink system attributes are important controlling factors of the canyon geomorphology, in particular:

(i) If the canyon exhibits an actual connection with a fluvial system [26];
(ii) If the canyon was connected to a river in the geological past and not now due to the actual sea level highstand phase or to the shifting of the river mouth [27–30];
(iii) If the canyon apex is located within 5 km of a fluvial outlet.

Several studies on the Dohrn canyon have been carried out, pointing out its important role in the volcanology of the Neapolitan area and the complexity of the seismic units related to its seismic stratigraphy [8,31–36]. Other studies, instead, have focused on the morpho-bathymetric setting of the Dohrn and Magnaghi canyons [34], on the relationships with the submarine gravity instabilities [37–39], and on the potential run-up and tsunami reconstructions from fossil submarine landslides [40]. The volcanic edifices of the Bay of Naples are aligned along a N10° tectonic lineament, following the Dohrn canyon and related to the Ortona-Roccamonfina line [39–46].

The aim of this paper is to analyze the dynamics of the sedimentary processes in the coastal areas of the Bay of Naples, in particular in the Naples canyons, by integrating the seismo-stratigraphic data with the sedimentological data. Previously published seismic sections have been reassessed [32,35] with the aim of reconstructing the Quaternary geologic evolution of the Naples canyons through seismo-stratigraphic knowledge. Ternary plots of the sedimentological data sampled at the seabed have been constructed, aimed at integration with the seismo-stratigraphic data.

The relationships between the individuation, the activity, and the geological developments of the Naples canyons and the great ignimbrite deposits of Naples, particularly the Campanian Ignimbrite (CI; 37 ky B.P.) [31,47–59] and the Neapolitan Yellow Tuff (NYT; 19 ky B.P.) [60–65], are herein discussed.

## 2. Geologic Setting

Naples Bay is an extensional basin located on the Eastern Tyrrhenian margin (Figure 1), which was created as an outcome of the extension parallel to the fold and thrust belt and related strike-slip and extensional tectonics, which have followed the anti-clockwise motion

of the Apennines and the growth of the oceanic lithosphere in the central Tyrrhenian basin. On the Campania continental margin, the peri-Tyrrhenian basins make up the extension of the coastal plains towards the sea, whose arrangement was controlled by extensional tectonics during the Plio-Quaternary [66–73]. Their tectono-sedimentary evolution was genetically related to the Neogene evolution of the Apenninic chain [74–79].

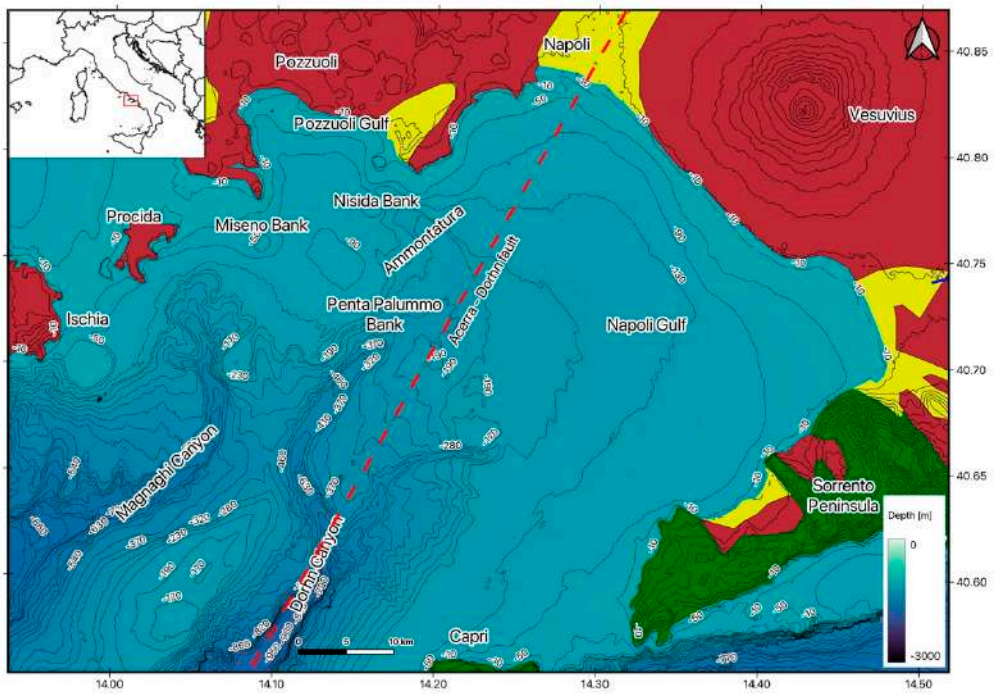


**Figure 1.** Geological sketch map of the study area. The location of the Acerra–Dohrn canyon fault has been reported.

In the Campania region, unconformable Quaternary basin fillings lie beneath the "internal" western tectonic structures of the Apennines, resulting from the propagation towards the sea of the outcropping tectonic units [79–81] (Figure 1). These units constitute the acoustic basement of the coastal basins and are made of either siliciclastic basin sequences or Meso-Cenozoic carbonates. Extensional tectonics concomitant with the uplift of the southern Apennines commenced in the early Pliocene and continued up to the middle-late Pleistocene, controlling the present-day physiography of the Campania Region.

On the Campania Plain, the first stage of lowering and flooding, early Pleistocene in age, was probably controlled by a NW–SE trending extensional phase, while the following stage, middle Pleistocene in age, responded mainly to a NE–SW extensional phase. The normal faults inherited from these stages were reactivated during the Late Pleistocene Holocene phases of subsidence and uplift, especially in the areas affected by volcano tectonics [68–73]. A strong volcanic aggradation occurred at 39 ky B.P. during the emplacement of the volcanic deposits of the Campanian Ignimbrite (39 ky B.P.) [47,59]. Due to the eruption of the Campanian Ignimbrite, the Campania Plain was completely emerged and was later controlled by the fluvial incision favored by the sea level lowering of the last glacial regression.

In western Naples Bay, the volcanic districts of the Procida, Vivara, and Ischia islands pertain to the Campi Flegrei volcanic district, including a number of submerged volcanoes [32,36,82–85]. This volcanic activity has controlled the formation and activity of the western branch of the Dohrn canyon and of the Magnaghi canyon, which drained the volcaniclastic input of the continental slope during the major eruptive phases. In eastern Naples Bay, the erosional and depositional processes on the continental shelf and slope during the Late Quaternary were influenced by the Somma–Vesuvius volcanic activity [80,83] and by the sedimentary processes on the Sarno–Sebeto coastal plain.

The coastal plain of the Sebeto river, on which the eastern part of the town of Naples lies, is located at the boundary of the Somma–Vesuvius volcanic complex and towards the Tyrrhenian coastline. The individuation of this plain has been triggered by a NE–SW-trending (counter Apenninic) normal fault, corresponding to the Acerra–Dohrn canyon fault (Figure 1), active after the eruption of the Campanian Ignimbrite and of the Neapolitan Yellow Tuff at 39 and 15 ky B.P., respectively [5,6,83–88].

A thick pyroclastic deposit with a trachytic and phonolitic composition related to a collapsed caldera is known as the Campanian Ignimbrite [31,47–59]. In this caldera, slight volcanic activity developed up to 1538 D.C. with the eruption of the Monte Nuovo volcanic edifice.

The Neapolitan Yellow Tuff (NYT) was deposited in the second phreato-magmatic eruption involving the Neapolitan area and outcrops over an area of 1000 $km^2$ [60–65]. The open quit quarries of the NYT deposits are found in the surrounding area of the old Naples town, (Capodimonte, Rione Sanita, Fontanelle, Camaldoli, Petraio, and Pizzofalcone). Due to the increasing urban development of Naples town, several quarries are located in the western sector of Campi Flegrei. These quarries have developed into many slope and trench quarries. NYT is composed of two members with distinct textures, dispersal trends, and volcanic compositions.

Romano et al. [89] showed new stratigraphic data on the Holocene landscape of Naples during the last 6 ky based on the geologic and archeological excavations collected during the public transport works. In particular, the samples used in this study were collected during the realization of the San Pasquale (SP) and Arco Mirelli (AM) metro stations under construction on Line 6 [85]. This study was carried out through an integrated geoarcheological approach based on the integration of facies analysis, tephrostratigraphy, archeology, and chronostratigraphic calibration. Four chronological stages have been distinguished, i.e., the prehistoric period (V–III millennium B.C.), the protostoric period (20th century B.C.–8th century B.C.), the Greek and Roman period (late 8th century B.C.–3rd century A.D.), and the Late Antiquity (4th–6th centuries A.D.), and the corresponding stratigraphic and volcanic deposits have been described.

Vacchi et al. [90] highlighted the millennial variability of the rates of sea level rise in the ancient harbor of Naples by using archeological, biostratigraphic, and isostatic constraints. The realization of the new underground railway of Naples town (Piazza Municipio) has allowed for the study of the harbor structures, showing fossil traces of biological indicators of previous sea levels. These data have been integrated with biostratigraphic data, providing new insights into the relative sea level evolution of the Naples harbor during recent geological times [91]. In particular, the biological assemblages found on the harbor structures have been analyzed (vermetids, *Ostrea* spp.), whose upper boundary of life shows the biological mean sea level. These proxies provide accurate relative sea level index points. The relative sea level evolution has been constrained starting from the Hellenistic period, when the relative sea level rose of about 2 mm/year, being controlled by the volcano–tectonic processes active in this area. Land-level changes caused an increase in negative land-level changes in the first two centuries BC and in the post-Antiquity period (i.e., since the fifth century AD). This trend of negative land-level changes was interrupted for five centuries, when a significant deceleration of the rising rate (0.2 mm/year) was observed. This stabilization of the relative sea level position is probably related to a positive bradyseism in Campi Flegrei.

## 3. Materials and Methods

Literature reviews, sedimentological data, and seismo-stratigraphic data were integrated to assess the geological development of the Naples canyons. In particular, the sea bottom samples considered in this paper for the study of the Naples canyons were recorded during oceanographic cruises performed by the CNR ISMAR of Naples, Italy, during the data acquisition of the CARG project of the Campania region (geological map n. 465 “Island of Procida”, scale 1:10,000, scale 1:50,000 [87]. In particular, we consider here the sea bottom

samples collected during the oceanographic cruises GMS98_01 (1998), GMS00_05 (2000), and GMSPM1 (2000) onboard the R/V Urania (National Research Council of Italy).

Figure 2 shows the DEM of the Naples Bay offshore area and the sketch geological map of Figure 1 onshore, with the superimposition of the location of the sea bottom samples and of the cores available in literature, which are useful to study the sedimentary dynamics of Naples Bay [91–93] and in particular of the Naples canyons [31,94,95].

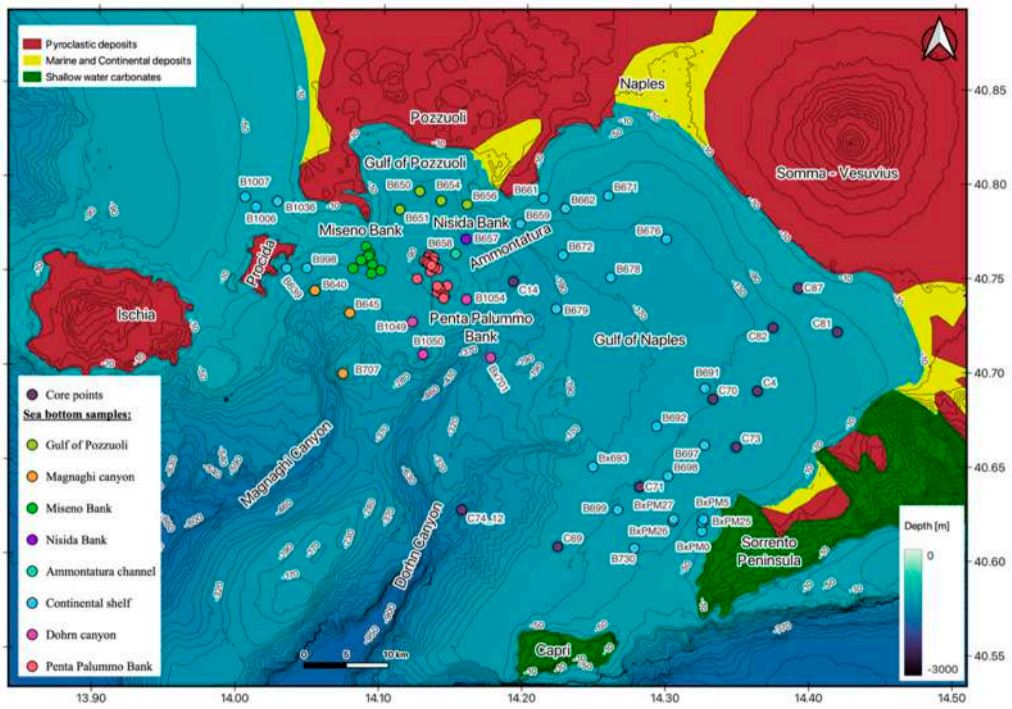


**Figure 2.** Sketch map of the sea bottom samples and cores.

The sedimentological data were plotted as ternary diagrams, both of clay–sand–silt and of gravel–sand–silt (due to the occurrence of a significant bioclastic component) using a sub-division in two main sets, from sample B1A2 to sample B1054 (first set) and from sample BXMIS1 to sample PM27 (second set) (Figure 2) [96]. Table 1 shows the different percentage of gravel, sand, silt, and shale and the grain size of the samples, as determined through the sedimentological analysis performed in the CNR ISMAR sedimentological laboratory. The laboratory sampling and the pre-treatment of the sediment samples were performed following the SNI procedure (DM 105 7/7/2008, par. 7). The sampling resolution was 50 cm thick stratigraphic intervals. The samples were stored at 4 °C and then treated with a solution of hydrogen peroxide. Then, the samples were washed with distilled water, dried at 40 °C, and weighed. The samples were wet-sieved using a sieve (63 µm) to perform the separation of the sandy fraction. The coarse-grained fraction of these deposits (>63 µm) was further separated into grain-size components by sieving at 0.5 phi intervals (ASTM series of sieves with meshes ranging from −2 to +4 115 phi). The pelitic fraction (<63 µm) was individuated using a laser particle sizer (Helos/Quixel Sympatec, Clausthall-Zehlleferd, Germany), in addition to the sedimentological laboratory (CNR ISMAR, Naples, Italy).

The sea bottom samples were further subdivided according to the base map of samples reported in Figure 2 with respect to their location, aiming at constructing detailed sedimentological maps of Naples Bay. Table 2 shows the sea bottom samples, their grain size, and their detailed location as a basic table for the construction of sedimentological maps in a GIS environment. This kind of work has allowed us to produce detailed sedimentological maps of the Pentapalummo and Miseno banks, of the slope surrounding the Dohrn and Magnaghi canyons, and of the continental shelf of Naples Bay.

**Table 1.** Sedimentological data of the sea bottom samples.

| Sea Bottom Sample | Gravel (%) | Sand (%) | Silt (%) | Shale (%) | Grain Size |
|---|---|---|---|---|---|
| 1A2 | 9.42 | 28.62 | 45.53 | 16.43 | Sandy silt |
| 1F2 | 7.30 | 77.29 | 10.43 | 4.98 | Silty sand |
| 1H2 | 6.61 | 34.36 | 38.06 | 20.97 | Sandy silt |
| 1J | 5.54 | 30.09 | 44.70 | 19.67 | Sandy silt |
| 1L | 7.11 | 42.40 | 35.35 | 15.14 | Sandy silt |
| 1M1 | 7.93 | 81.15 | 7.69 | 3.22 | Silty sand |
| e1R | 8.86 | 36.37 | 36.98 | 17.78 | Sandy silt |
| 1V | 7.57 | 89.21 | 2.60 | 0.62 | Sand |
| 1W | 10.37 | 85.51 | 2.96 | 1.16 | Sand |
| 1Y | 17.09 | 75.69 | 5.27 | 1.95 | Sand |
| BX7_1 | 0.00 | 57.82 | 42.18 | 0.00 | Silty sand |
| B639 | 0.20 | 11.13 | 64.91 | 23.76 | Sandy silt |
| B640 | 0.00 | 2.12 | 68.48 | 29.40 | Silt |
| B644 | 0.13 | 9.88 | 67.16 | 22.82 | Silt |
| B645 | 0.00 | 10.25 | 58.61 | 31.14 | Sandy silt |
| B650 | 0.02 | 3.83 | 68.96 | 27.20 | Silt |
| B651 | 0.03 | 7.71 | 71.62 | 20.64 | Silt |
| B654 | 0.08 | 14.86 | 65.23 | 19.83 | Sandy silt |
| B656 | 57.58 | 35.43 | 5.04 | 1.95 | Gravel sand |
| B657 | 0.51 | 31.07 | 50.44 | 17.97 | Sandy silt |
| B658 | 0.21 | 2.82 | 70.22 | 26.75 | Silt |
| B659 | 0.00 | 19.93 | 63.98 | 16.09 | Sandy silt |
| B661 | 1.16 | 35.39 | 51.43 | 12.01 | Sandy silt |
| B662 | 8.93 | 21.53 | 55.96 | 13.58 | Sandy silt |
| B671 | 2.01 | 40.94 | 44.66 | 12.39 | Sandy silt |
| B672 | 0.15 | 3.09 | 59.77 | 36.99 | Silt |
| B676 | 0.18 | 7.99 | 67.33 | 24.51 | Silt |
| B678 | 0.00 | 8.87 | 56.67 | 34.45 | Silt |
| B679 | 0.15 | 3.09 | 59.77 | 36.99 | Silt |
| B691 | 0.00 | 14.31 | 56.78 | 28.91 | Sandy silt |
| B692 | 0.05 | 15.86 | 52.62 | 31.46 | Sandy silt |
| Bx693 | 0.00 | 17.23 | 53.30 | 29.48 | Sandy silt |
| B697 | 0.00 | 14.24 | 57.99 | 27.77 | Sandy silt |
| B698 | 0.00 | 8.71 | 55.92 | 35.37 | Silt |
| B699 | 0.00 | 15.82 | 43.51 | 40.67 | Sandy silt |
| Bx701 | 0.20 | 8.19 | 56.22 | 35.39 | Silt |
| B707 | 0.28 | 3.10 | 52.28 | 44.34 | Silt |
| B730 | 1.79 | 52.45 | 30.43 | 15.33 | Silty sand |
| B972 | 6.97 | 32.15 | 52.86 | 8.02 | Sandy silt |
| B973 | 0.00 | 33.43 | 59.36 | 7.21 | Sandy silt |
| B979 | 0.00 | 54.73 | 41.11 | 4.16 | Silty sand |

**Table 1.** *Cont.*

| Sea Bottom Sample | Gravel (%) | Sand (%) | Silt (%) | Shale (%) | Grain Size |
|---|---|---|---|---|---|
| B981 | 0.00 | 94.49 | 3.86 | 1.66 | Sand |
| B987 | 0.00 | 31.73 | 61.86 | 6.41 | Sandy silt |
| Bx990 | 0.00 | 11.95 | 66.09 | 21.97 | Sandy silt |
| B992 | 17.92 | 71.95 | 7.46 | 2.66 | Sand |
| B993 | 0.79 | 33.63 | 51.57 | 14.02 | Sandy silt |
| B994 | 1.94 | 25.01 | 55.84 | 17.21 | Sandy silt |
| B998 | 0.32 | 10.25 | 63.04 | 26.40 | Sandy silt |
| B1006 | 0.74 | 33.95 | 51.96 | 13.35 | Sandy silt |
| B1007 | 0.67 | 13.67 | 64.46 | 21.20 | Sandy silt |
| B1036 | 1.92 | 77.50 | 14.71 | 5.87 | Silty sand |
| B1044 | 1.28 | 45.75 | 42.56 | 10.41 | Sandy silt |
| B1049 | 2.70 | 21.02 | 53.46 | 22.82 | Sandy silt |
| B1050 | 12.46 | 62.36 | 14.66 | 10.53 | Silty sand |
| B1054 | 11.19 | 26.95 | 43.37 | 18.49 | Sandy silt |
| BxMIS1 | 0.00 | 33.34 | 66.66 | 0.00 | Sandy silt |
| BxMIS2 | 4.26 | 90.33 | 5.41 | 0.00 | Sand |
| BxMIS3 | 0.85 | 93.55 | 5.60 | 0.00 | Sand |
| BxP_2 | 8.14 | 63.03 | 28.83 | 0.00 | Silty sand |
| BxP_3 | 18.37 | 77.27 | 4.36 | 0.00 | Sand |
| BxP_5 | 0.51 | 81.44 | 18.05 | 0.00 | Silty sand |
| BxPM0 | 0.34 | 91.27 | 8.39 | 0.00 | Sand |
| BxPM5 | 0.00 | 96.29 | 3.71 | 0.00 | Sand |
| BxPM25 | 6.66 | 69.45 | 23.89 | 0.00 | Silty sand |
| BxPM26 | 2.26 | 76.08 | 21.67 | 0.00 | Silty sand |
| BxPM27 | 3.99 | 52.17 | 43.83 | 0.00 | Silty sand |

**Table 2.** Detailed location data and grain size of the sea bottom samples.

| Sample | Grain Size | Detailed Location (Naples Bay) |
|---|---|---|
| 1A2 | Sandy silt | Pentapalummo Bank |
| 1H2 | Sandy silt | Pentapalummo Bank |
| 1J | Sandy silt | Pentapalummo Bank |
| 1L | Sandy silt | Pentapalummo Bank |
| 1M1 | Silty sand | Pentapalummo Bank |
| 1R | Sandy silt | Pentapalummo Bank |
| 1V | Sand | Pentapalummo Bank |
| 1W | Sand | Pentapalummo Bank |
| 1Y | Sand | Pentapalummo Bank |
| BX7_1 | Silty sand | Continental shelf of Naples Bay |
| B639 | Sandy silt | Continental shelf of Naples Bay |
| B640 | Silt | Head of the Magnaghi canyon |

**Table 2.** *Cont.*

| Sample | Grain Size | Detailed Location (Naples Bay) |
|---|---|---|
| B644 | Silt | Continental shelf of Naples Bay |
| B645 | Sandy silt | Head of the Magnaghi canyon |
| B650 | Silt | Gulf of Pozzuoli |
| B651 | Silt | Gulf of Pozzuoli |
| B654 | Sandy silt | Gulf of Pozzuoli |
| B656 | Gravel sand | Gulf of Pozzuoli |
| B657 | Sandy silt | Nisida Bank |
| B658 | Silt | Slope westwards of the Ammontatura channel |
| B659 | Sandy silt | Continental shelf of Naples Bay |
| B661 | Sandy silt | Continental shelf of Naples Bay |
| B662 | Sandy silt | Continental shelf of Naples Bay |
| B671 | Sandy silt | Continental shelf of Naples Bay |
| B672 | Silt | Continental shelf of Naples Bay |
| B676 | Silt | Continental shelf of Naples Bay |
| B678 | Silt | Continental shelf of Naples Bay |
| B679 | Silt | Continental shelf of Naples Bay |
| B691 | Sandy silt | Continental shelf of Naples Bay |
| B692 | Sandy silt | Continental shelf of Naples Bay |
| Bx693 | Sandy silt | Continental shelf of Naples Bay (next to the head of the Dohrn eastern branch) |
| B697 | Sandy silt | Continental shelf of Naples Bay |
| B698 | Silt | Continental shelf of Naples Bay |
| B699 | Sandy silt | Continental shelf of Naples Bay |
| Bx701 | Silt | Dohrn western branch |
| B707 | Silt | Magnaghi canyon |
| B730 | Silty sand | Continental shelf of Naples Bay |
| B972 | Sandy silt | Continental shelf of Naples Bay |
| B973 | Sandy silt | Continental shelf of Naples Bay |
| B979 | Silty sand | Continental shelf of Naples Bay |
| B981 | Sand | Continental shelf of Naples Bay |
| B987 | Sandy silt | Continental shelf of Naples Bay |
| Bx990 | Sandy silt | Continental shelf of Naples Bay |
| B992 | Sand | Continental shelf of Naples Bay (northwards of the Magnaghi canyon) |
| B993 | Sandy silt | Continental shelf of Naples Bay (northwards of the Magnaghi canyon) |
| B994 | Sandy silt | Continental shelf of Naples Bay (northwards of the Magnaghi canyon) |
| B998 | Sandy silt | Continental shelf of Naples Bay (offshore Procida Island) |

**Table 2.** *Cont.*

| Sample | Grain Size | Detailed Location (Naples Bay) |
|---|---|---|
| B1006 | Sandy silt | Continental shelf of Naples Bay (offshore Procida Island) |
| B1007 | Sandy silt | Continental shelf of Naples Bay (offshore Procida Island) |
| B1036 | Silty sand | Continental shelf of Naples Bay (offshore Procida Island) |
| B1044 | Sandy silt | Continental shelf of Naples Bay |
| B1049 | Sandy silt | Dohrn western branch |
| B1050 | Silty sand | Dohrn western branch |
| B1054 | Sandy silt | Dohrn western branch |
| BxMIS1 | Sandy silt | Miseno Bank |
| BxMIS2 | Sand | Miseno Bank |
| BxMIS3 | Sand | Miseno Bank |
| BxP_2 | Silty sand | Continental shelf of Naples Bay |
| BxP_3 | Sand | Continental shelf of Naples Bay |
| BxP_5 | Silty sand | Continental shelf of Naples Bay |
| BxPM0 | Sand | Continental shelf of Naples Bay |
| BxPM5 | Sand | Continental shelf of Naples Bay |
| BxPM25 | Silty sand | Continental shelf of Naples Bay |
| BxPM26 | Silty sand | Continental shelf of Naples Bay |
| BxPM27 | Silty sand | Continental shelf of Naples Bay |

Core data previously analyzed in Naples Bay [92,93], and in particular in the Naples canyons [31] and the Ammontatura Channel [94], were reassessed in order to highlight the influence of Quaternary sedimentation, as detected by the cores, on the development of the Naples canyons. Table 3 shows the characteristics of the analyzed cores of the Bay of Naples, while their location is shown in Figures 2 and 3.

**Table 3.** Characteristics of the core data reinterpreted in this paper.

| Core | Location | Reference |
|---|---|---|
| C69 | Naples Bay | Sacchi et al. [92]; Molisso et al. [93] |
| C71 | Naples Bay | Sacchi et al. [92]; Molisso et al. [93] |
| C73 | Naples Bay | Sacchi et al. [92]; Molisso et al. [93] |
| C70 | Naples Bay | Sacchi et al. [92]; Molisso et al. [93] |
| C4 | Naples Bay | Sacchi et al. [92] |
| C82 | Naples Bay | Sacchi et al. [92]; Molisso et al. [93] |
| C81 | Naples Bay | Sacchi et al. [92] |
| C87 | Naples Bay | Molisso et al. [93] |
| C74_12 | Naples canyons | Aiello et al. [31] |
| C14 | Ammontatura Channel | Insinga et al. [94] |

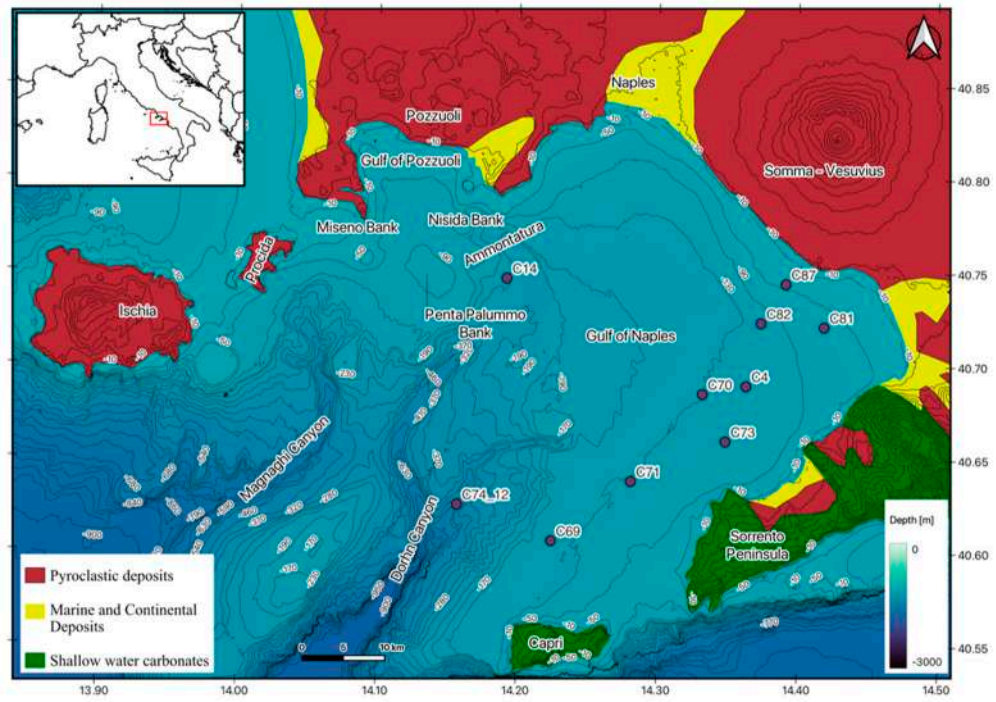


**Figure 3.** Sketch map of the analyzed cores (see Table 3 for further information on the cores).

Sparker seismic sections located in Naples Bay and previously published by Fusi et al. [32] were re-interpreted, aimed at collecting new seismo-stratigraphic evidence on the geological evolution of the Naples canyons. Sparker data were recorded by the Istituto Universitario Navale (now Parthenope University of Naples, Italy) by using a Multispot Extended Array Sparker system [32]. The seismic sections were recorded graphically on continuous paper sheets. The vertical scales ranged between 1 and 2 s, while the vertical resolution was about 6 m.

A detailed interpretation of the NAM3 multichannel seismic profile is herein shown [35], which is one of the seismic sections supporting the geological sheet n. 465 "Isola di Procida" [35]. The NAM3 seismic profile was recorded through an Airgun seismic source [35]. Moreover, some seismic sections, recorded in the GMS00_05 oceanographic cruise (R/V Urania, National Research Council of Italy) through a Watergun seismic source, and previously published by Aiello et al. [95] were re-interpreted, aimed at collecting seismo-stratigraphic evidence on the Naples canyons.

Significant sub-bottom Chirp profiles of Naples Bay were selected in order to give new insights into the geological evolution of the Naples canyons. The Chirp data were recorded during the oceanographic cruises GMS97-01, GMS98-01, and GMS00_05, carried out by the CNR-ISMAR of Naples, Italy, onboard the R/V Urania (National Research Council of Italy).

## 4. Results

### *4.1. Morpho-Bathymetric Data*

Some bathymetric profiles were constructed in order to highlight the morphology of the Naples canyons. A sketch DEM reporting the location of the bathymetric profiles crossing the Naples canyon system is reported in Figure 4. A multibeam bathymetric dataset was previously acquired as part of the CARG project of the Naples and Salerno bays (http://www.isprambiente.gov.it/Media/carg/campania.html, accessed on 11 April 2022; Figure 4) [35].

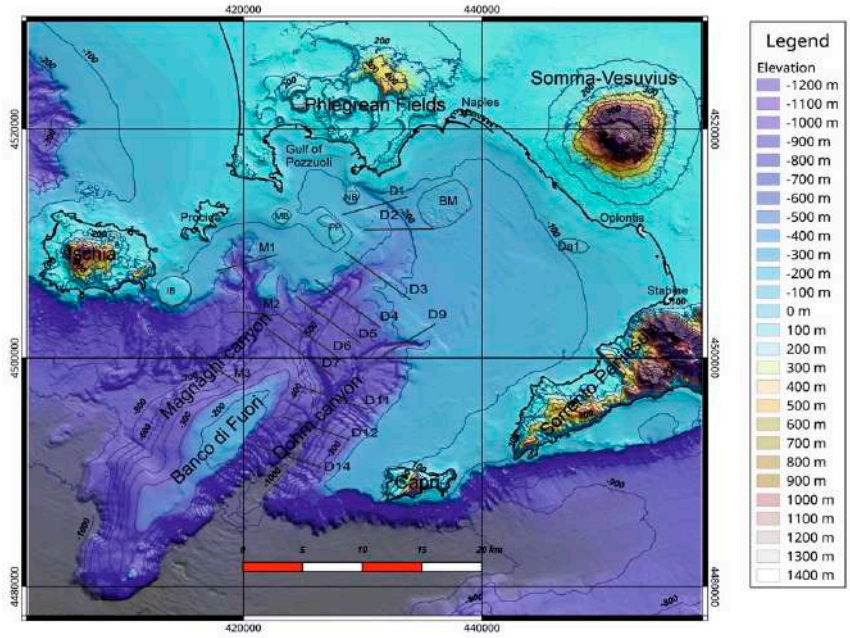


**Figure 4.** DEM of Naples Bay reporting the location of the bathymetric profiles shown in this paper. Dohrn canyon: D1, D2, D3, D4, D5, D6, D7, D9, D11, D12, D14; Magnaghi canyon: M1, M3, M5. Da1: debris avalanche deposits offshore Somma–Vesuvius; BM: Banco della Montagna. The Dohrn canyon, the Magnaghi canyon, and the Banco di Fuori morpho-structural high are also reported.

The DEM (Digital Elevation Model) merged both onshore and offshore data and was previously used as a base in other papers [82]. Onshore data show the morphological settings of the Somma–Vesuvius, Campi Flegrei, Ischia, and Capri islands, as well as the Sorrento Peninsula (Figure 4). The canyon system of Naples Bay starts from the shelf break, located along the isobath of 140 m. The regional morphologic setting of the canyon system is controlled by two main morpho-structural lineaments, the Banco di Fuori, bounding southwards, and the Capri high, bounding eastwards, in correspondence with the bathyal plain. Eleven bathymetric profiles cross the Dohrn system (D1, D2, D3, D4, D5, D6, D7, D9, D11, D12, D14; Figure 4), while three bathymetric profiles cross the Magnaghi system (M1, M3, M5; Figure 4).

The dimension of the Dohrn submarine ranges between several hundred meters and more than one kilometer, its extent ranges from 250 m at the shelf margin to 1300 m at the spot with the bathyal water depths, while the gradient of its slopes reaches 35° in the steep-sided sectors (Figure 4). The Dohrn submarine is characterized by major curved branches, the western one and the eastern one (Figure 4). Towards the continental shelf, the western branch merges into the shelf through a palaeo-channel ("Ammontatura" channel; Figures S1 and S2), whose origin is correlated with the hydrodynamic regime driven by the northern axis of the Dohrn canyon. Its development post-dates the latest stages of erosion and transport in the canyon and pre-dates the formation of the most recent volcanic edifices in the Gulf of Pozzuoli, as suggested by its abrupt termination towards the Nisida bank.

The interpretation of bathymetric profiles shows the distribution of the V-shaped erosional profiles with respect to the U-shaped depositional profiles in the whole canyon system (Figures S1–S5). V-shaped erosional profiles are prevalent in both branches of the canyon (profiles D3, D4, D7, D9, D11, and D12; Figures S1–S4). The U-shaped depositional morphologies, suggesting recent phases of canyon filling, are singled out in the largest, central part of the Dohrn western branch and in the lower part of the canyon's main thalweg (Figures S1, S2 and S4).

The bathymetric profiles located along the Dohrn western branch suggest the occurrence of slide scars (Figure S1). Round-shaped morphologies, located on the thalweg of the canyon, are interpreted as inselberg-type structures and probably originated from

morpho-selective erosion acting along the canyon's valley (bathymetric profiles D5 and D7; Figures S1 and S3). The section D3 (Figure S1), crossing the retreating canyon's head, shows terrace rims located at water depths of 340 m and 300 m. This morphological evidence suggests at least two phases in the activity and the retreatment of the canyon's head. Well-developed terrace rims, at least five rims, are recognized in the bathymetric profile D6 (Figure S2), located at water depths of 400 m, 380 m, and 350 m.

The erosion and the transport of the volcanoclastic input in the western sector of the gulf (offshore the Ischia and Procida islands) acts along the axis of the Magnaghi canyon, which appears unrelated to present or past fluvial drainage system on land. Its head is typically trilobate with three main tributary channels joining basinwards into the main axis (Figure 4). The bathymetric profiles cross the canyon's head, the central sector of the canyon, and the terminal sector of the canyon (Figure S5). In particular, the bathymetric profile M1 displays the tributary channels feeding the canyon. V-shaped erosional profiles prevail in the canyon's head and in the central sector of the canyon, while U-shaped depositional profiles can be observed in the terminal sector of the canyon.

### *4.2. Sedimentological Data*

A ternary plot, ternary graph, triangle plot, simplex plot, Gibbs triangle or de Finetti diagram is a barycentric plot of three variables that sum to a constant. It graphically shows the ratios of the three variables as positions in an equilateral triangle. It is used in sedimentological studies to show the compositions of systems composed of three species.

Six ternary plots of the sedimentological data were constructed by using the free software Ternary Plot, available online (https://www.ternaryplot.com/, accessed on 27 July 2023). We added the grain size of the gravel of the sea bottom samples to the grain size of the sand and considered as the variables of the triangle diagram: sand + gravel, silt, and shale (Figures 5–7). The ternary plots of the sedimentological data were constructed taking into account the location of sea bottom samples reported in Table 2. The ternary plots of the continental shelf of Naples Bay (Figure 5), of the Miseno and Nisida banks (Figure 5), of the Pentapalummo Bank (Figure 6), of the Gulf of Pozzuoli (Figure 6), and of the Naples canyons (Dohrn and Magnaghi; Figure 7) are herein shown.

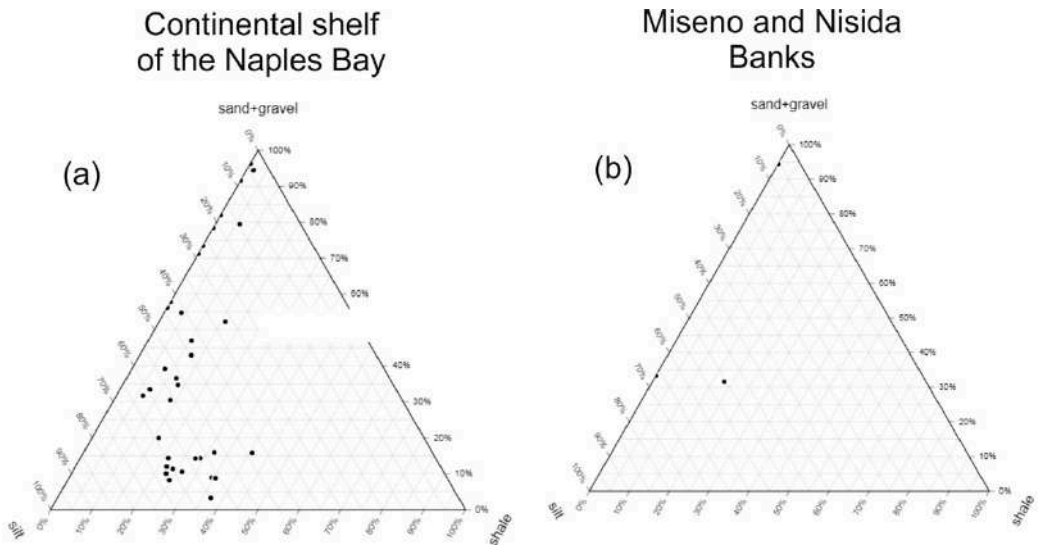


**Figure 5.** Ternary plots of the sedimentological data of the sea bottom samples on the continental shelf of Naples Bay (**a**) and of the Miseno and Nisida banks (**b**). The location of samples is reported in Figure 2. Continental shelf of Naples Bay (**a**): BX7_1, B639, B659, B661, B662, B671, B672, B676, B678, B679, B691, B692, B697, B698, B699, B730, B972, B973, B979, B981, B987, B998, B1006, B1007, B1036, Bx990, B1044, BxP_2, BxP_3, BxP_5, BxPM0, BxPM5, BxPM25, BxPM26, BxPM27. Miseno and Nisida banks (**b**): BxMIS1, BxMIS2, BxMIS3, B657.

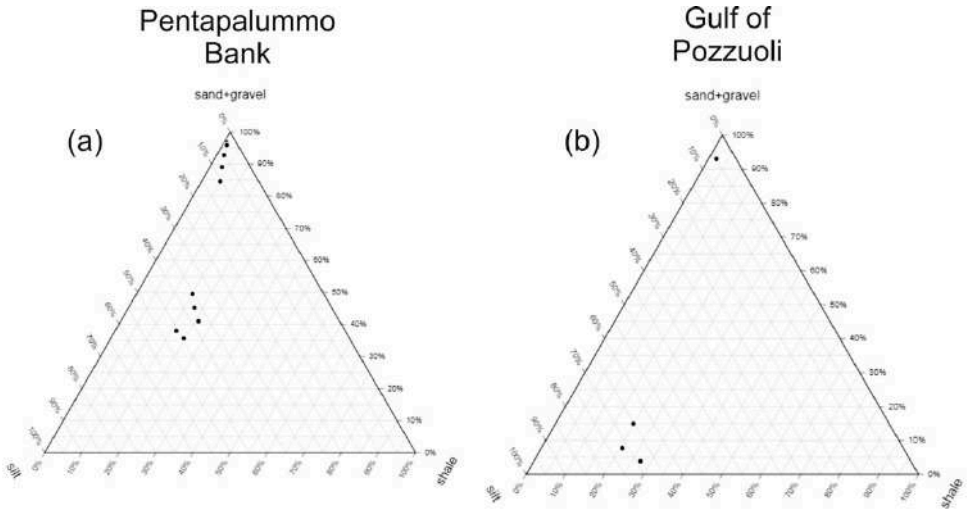


**Figure 6.** Ternary plots of the sedimentological data of the sea bottom samples from the Pentapalummo Bank (**a**) and the Gulf of Pozzuoli (**b**). The location of the samples is reported in Figure 2. Pentapalummo Bank (**a**): 1A2, 1F2, 1H2, 1J, 1L, 1M1, 1R, 1V, 1W, 1Y. Gulf of Pozzuoli (**b**): B650, B651, B654, B656.

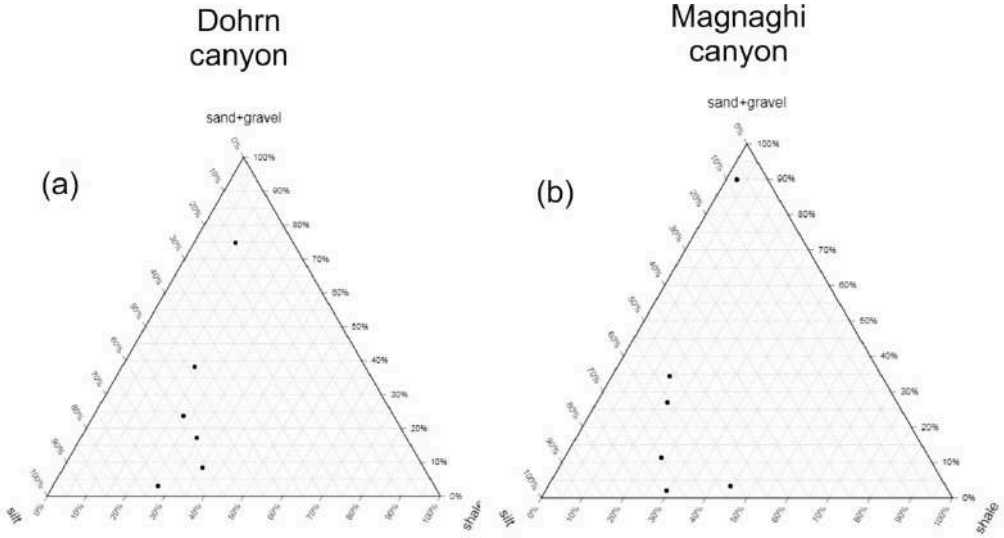


**Figure 7.** Ternary plots of the sedimentological data of the sea bottom samples in the Dohrn canyon (**a**) and the Magnaghi canyon (**b**). The location of samples is reported in Figure 2. Dohrn canyon (**a**): B658, Bx693, Bx701, B1049, B1050, B1054. Magnaghi canyon (**b**): B640, B645, B707, B992, B993, B994.

The ternary plot of the continental shelf of Naples Bay displays three subsets of textures (Figure 5a). The first subset is characterized by a percentage of sand + gravel ranging between 70% and 100% and a percentage of silt ranging between 0% and 30%. These are silty sands with subordinate fractions of gravel, bioclastic in origin. The second subset is characterized by a percentage of silt from 45% to 65% and that of shale from 10% to 20%, while the remaining component is represented by sand + gravel (Figure 5a). These are shale silts, with a very high subordinate component of sand + gravel. The third subset is distinguished by a percentage of silt from 80% to 100%, a percentage of shale from 20% to 45%, and a percentage of sand and gravel from 5% to 20% (Figure 5a). These are sandy silts, also including a shale fraction. Subordinate sedimentological data were obtained from scattered outcrops on the Miseno and Nisida banks, showing a percentage of sand + gravel of 95% associated with a percentage of silt of 5%. This suggests the occurrence of bioclastic sands on the two banks (Figure 5b).

Ternary plots of the Pentapalummo Bank and of the Gulf of Pozzuoli were also constructed (Figure 6a,b). On the Pentapalummo Bank, two subsets of samples can be distinguished (Figure 6a). The first subset of samples is characterized by a percentage of sand + gravel from 80% to 100%, while a percentage of silt ranges from 10% to 20%. These are bioclastic sands with a subordinate silty component. The second subset of samples is characterized by a percentage of silt from 60% to 40%, while the shale percentage ranges between 30% and 40% (Figure 6a). These are shale silts, with a very high subordinate percentage of sand + gravel. In the Gulf of Pozzuoli, a single sample has a high percentage of sand + gravel, and the occurrence of bioclastic sands can be assumed. Three other samples are characterized by a percentage of silt from 85% to 95% and by a percentage of shale from 15% to 5% (Figure 6b). These are composed of shale silts.

Ternary plots of the Naples canyons were constructed (Figure 7a,b). The ternary plot of the Dohrn canyon shows that a single sample is characterized by a percentage of sand + gravel of 75% and by a percentage of silt of 25% (Figure 7a). It is characterized as a silty bioclastic sand. Other samples are characterized by a percentage of silt from 30% to 40%, by a percentage of sand + gravel from 10% to 40%, and by a percentage of shale from 30% to 40%. The ternary plot of the Magnaghi canyon shows that a single sample in the upper part of the diagram has a percentage of sand + gravel of 90%, and the occurrence of coarse-grained deposits may be inferred. Other samples are characterized by a percentage of sand + gravel up to 90% and by a percentage of silt from 60% to 100% (Figure 7b).

Detailed sedimentological maps were constructed based on the data of the sea bottom samples, focusing on the different areas of the Gulf of Naples (Figures S6–S9). Figure S6 shows the division of the sea bottom samples in different sub-areas of the Gulf of Naples, including the continental shelf of Naples Bay, the Gulf of Pozzuoli, the Dohrn and Magnaghi canyons, the Miseno Bank, the Nisida Bank, and the Penta Palummo Bank.

A sedimentological map showing the distribution of the sands in Naples Bay and particularly on the Phlegrean banks (Miseno, Nisida, and Pentapalummo) was constructed (Figure S7). The sands are mainly located on the Pentapalummo and Miseno banks, with only one sample detected the sands on the Nisida Bank. Based on these data and on our previous papers, these are bioclastic sands, widespread on the Phlegrean banks [97,98]. Aiello and Caccavale [96] highlighted the importance of the bioclastic carbonate sedimentation in Naples Bay, showing that a model of mixed carbonate–siliciclastic sedimentation may be applied. A transition from bioclastic to siliciclastic deposits exists, starting from the northern Ischia offshore (bioclastic) to the Gulf of Pozzuoli (siliciclastic) [98]. The sedimentological data shown in Figure S7 confirm the importance of the bioclastic sands in the Bay of Naples.

Two sedimentological maps showing the distribution of the sandy silts and silty sands in the Bay of Naples were also constructed (Figures S8 and S9). This facies is very extended and widespread in the gulf, extending from the continental shelf offshore the Sorrento Peninsula towards the offshore of Naples town, the Phlegrean banks, and the Procida offshore area (Figure S8).

The sandy silts and silty sands are interpreted as a sandy facies, characteristic of the coastal areas of Naples Bay (Figures S8 and S9). Similar facies have been observed in the Adriatic offshore [97], where sedimentological and geochemical data have been presented. Droghini [97] showed that the sandy facies of the Adriatic offshore occurs as a coastal wedge and is composed of sandy–silty sediments, enriched in silica, between the Gargano Promontory and Pescara and Termoli.

Moreover, we reassessed significant core data of the Bay of Naples that were previously published in order to use litho-stratigraphic core data useful for the geological development of the Naples canyons [29,88–90]. We individuated these cores based on a literature review [31,92–94]. A stratigraphic section was constructed (Figure 8) through the reassessment of the stratigraphic data [92] regarding the gravity cores C69, C71, C73, C70, C4, C82, and C81.

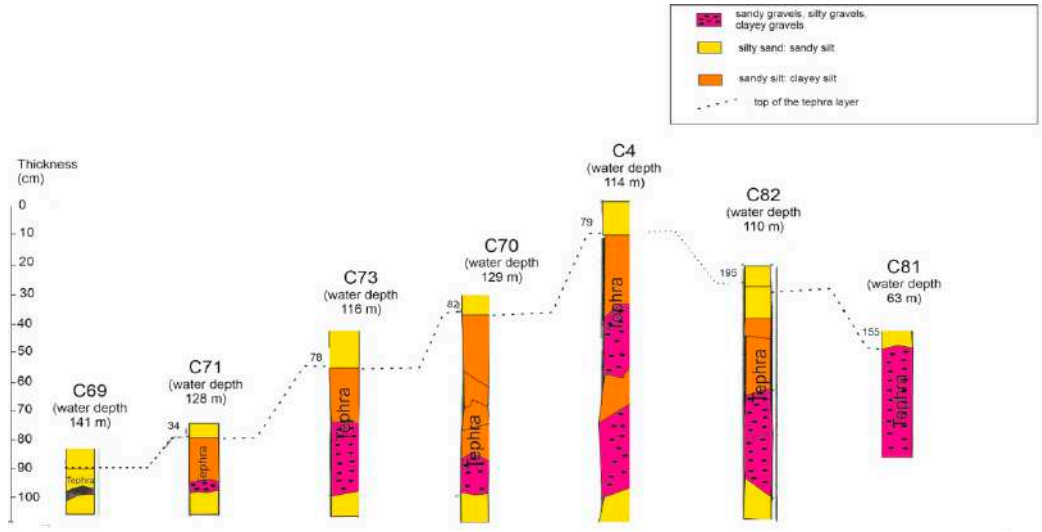


**Figure 8.** Stratigraphic sections of the core data C69, C71, C73, C70, C4, C82, and C81 in the Bay of Naples (modified after Sacchi et al. [92]). The location of the cores is reported in Figures 2 and 3.

Naples Bay has gravity cores at water depths between 63 m and 141 m, which provide a transect across the bay. The length of the recovered core sections ranges from 584 cm for core C82 to 176 cm for core C71. The core samples represent stratigraphic successions of the last few thousand years towards the mid-inner shelf but may also reach the base of the Holocene off the shelf break. The core data display the 79 AD Vesuvius tephra, as interlayered in the Quaternary marine deposits (Figures 9 and 10) [92], whose thickness ranges between 90 and 40 cm next to the Sarno Plain (C81, C82, C4) and 10 cm next to the shelf break of Naples Bay (C69) (Figure 9). As shown in Figure 9, the tephra underlies older Quaternary marine deposits, composed of sandy silts, whose top is marked by an erosional surface and is overlain, in turn, by younger marine deposits. The tephra deposits are different in the proximal areas (coarse-to-medium grained sands and gravels) with respect to the distal ones (sandy silts with fine-grained lithic and bioclastic components) [92] (Figures 9 and 10). The tephra deposits, as detected in the gravity cores, have different characteristics compared with the corresponding deposits detected onshore in the Somma–Vesuvius volcanic complex [82].

### *4.3. Seismo-Stratigraphic Data*

In this paper, we have reassessed some seismic sections that were previously published (see [32]), with the aim to improve the seismo-stratigraphic knowledge of the Bay of Naples (Figures 11–14). The reflector pattern and the seismic attributes, as the amplitude and continuity, are used to perform the geological interpretation of the seismic sections. Moreover, the reflector patterns are used to support the geological interpretation (e.g., inclined reflectors as indicators for prograding sedimentary bodies, incised valleys as indicators for sea level fall, etc.).

The bounding surfaces of the seismic units are defined based on the external geometry and on the internal reflector patterns, more than the recognition of the corresponding seismic facies (acoustically transparent seismic facies for volcanic seismic units, highly continuous and parallel seismic reflectors as Holocene marine deposits, and so on). Sea bottom multiples and ringing in the seismic sections are also indicated (Figures 11–14).

In particular, the seismic profile 1990-05 shows the seismo-stratigraphic architecture of the Bay of Naples between the Ammontatura channel and the Pentapalummo Bank (Figure 11). Based on the above seismo-stratigraphic criteria, seven seismic units are recognized. Inclined reflectors are interpreted as prograding sedimentary bodies of the Early–Middle Pleistocene prograding wedge (1 in Figure 11). The top of seismic unit 1 represents a regional unconformity, overlain by the seismic reflectors of unit 2 with onlap

(Figure 11). Based on the observed stratigraphic relationships and on the seismic facies, characterized by progradational reflectors, less inclined than the prograding reflectors of unit 1, unit 2 is interpreted as a Middle Pleistocene transgressive sequence, as shown by the onlap on the underlying seismic unit. It separates the two progradational wedges, i.e., the Early Pleistocene and Late Pleistocene (unit 3), representing the stratigraphic bulk of Naples Bay (Figure 11).

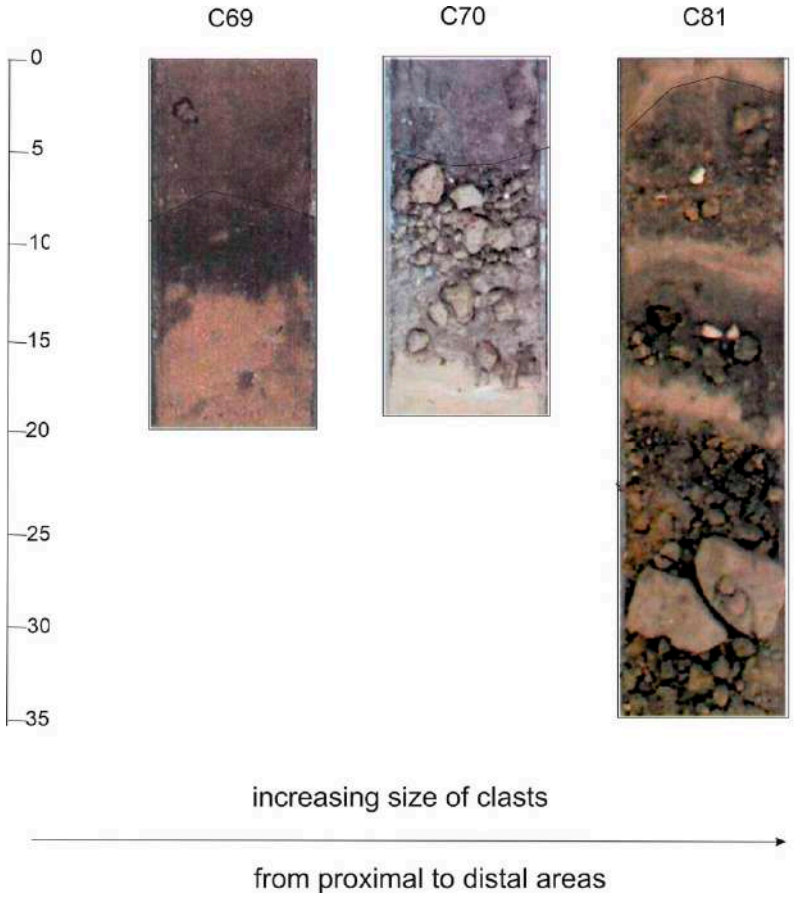


**Figure 9.** Detailed stratigraphic data of the C69, C70, and C81 cores showing the increasing size of clasts from proximal to distal areas (modified after Sacchi et al. [92]). The location of the cores is reported in Figures 2 and 3.

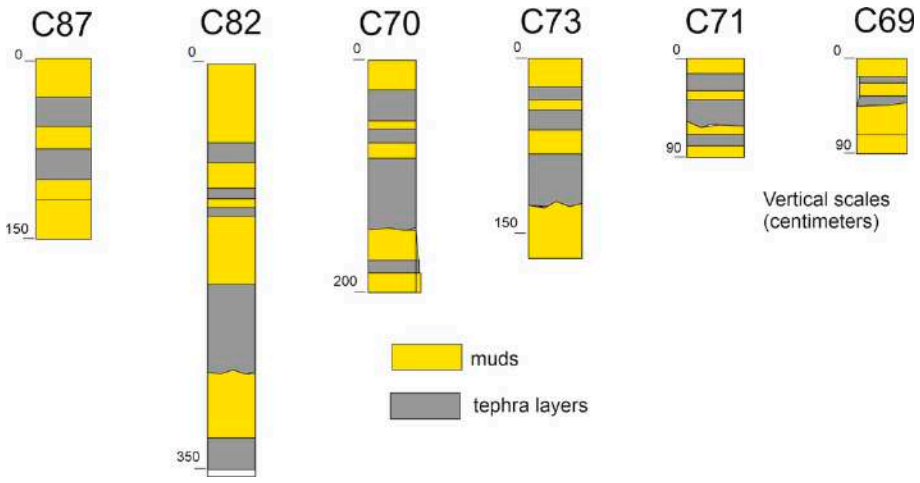


**Figure 10.** Stratigraphic sections of the C87, C82, C70, C73, C71, and C69 cores (modified after Molisso et al. [93]). The location of the cores is reported in Figures 2 and 3.

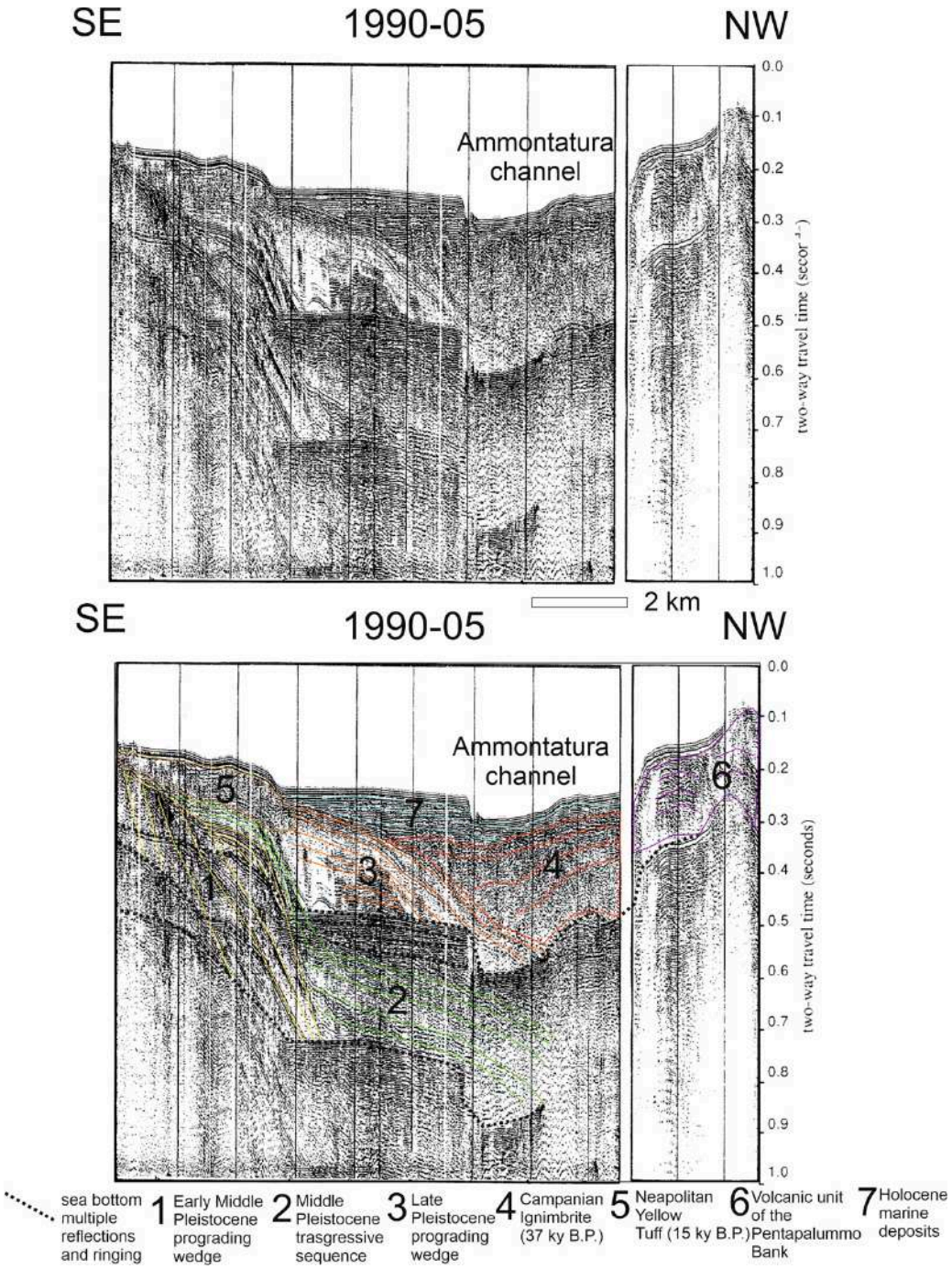


**Figure 11.** Seismic profile 1990-05 and corresponding geologic interpretation (modified after Fusi et al. [32]).

Unit 4 is characterized by an acoustically transparent seismic facies and overlies with onlap the top of seismic unit 3, interpreted as the Late Pleistocene prograding wedge. This unit has been interpreted as the Campanian Ignimbrite (CI), an important volcanic unit of the Campania Plain and of the Naples area, dated to 37 ky B.P. based on the geological literature of the area. It is a wedge-shaped seismic unit, whose seismic aspect is very characteristic, being acoustically transparent, as a general rule, provided some scattered seismic reflectors appear locally (Figure 11).

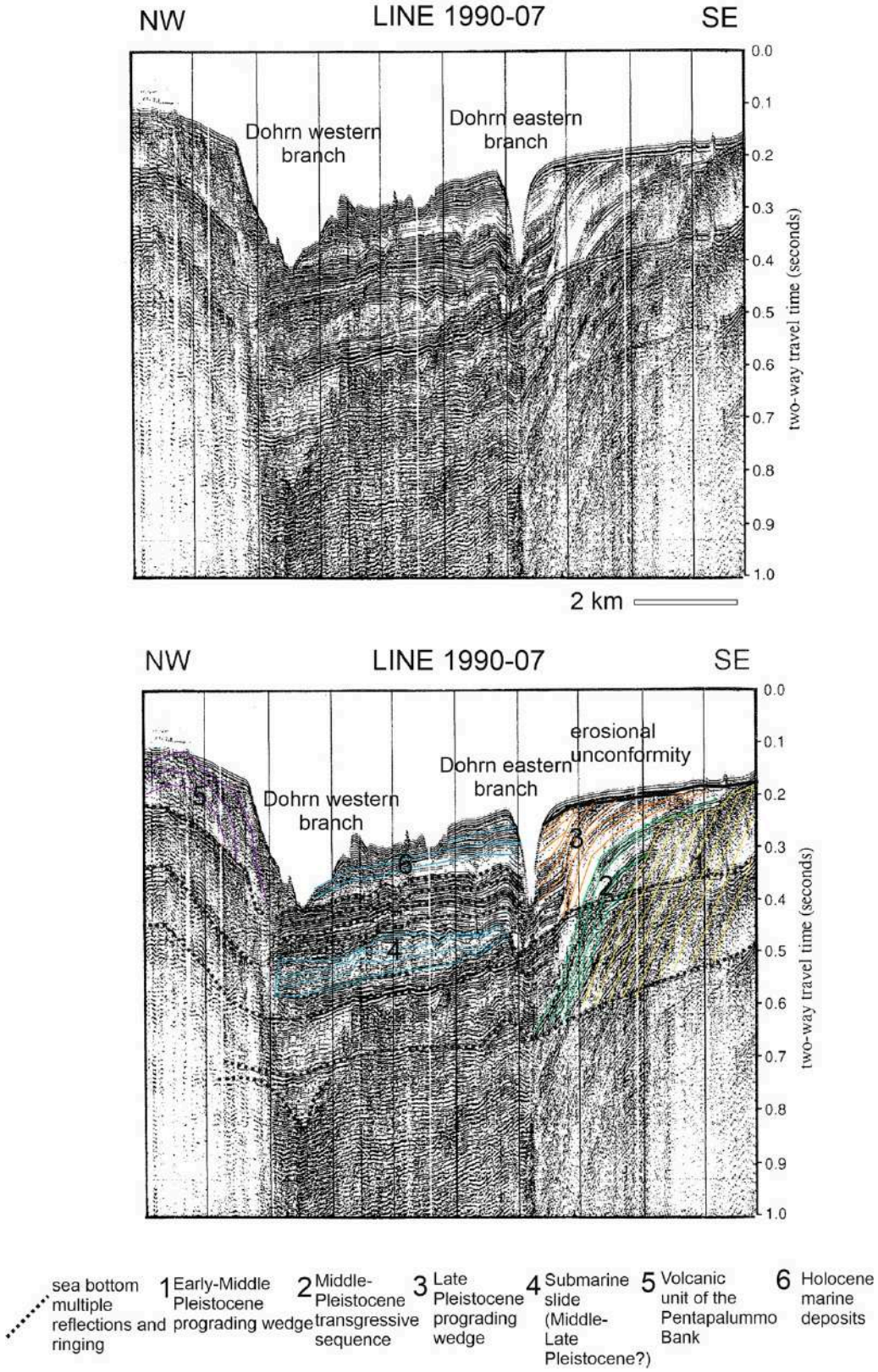


**Figure 12.** Seismic profile 1990–07 and corresponding geologic interpretation (modified after Fusi et al. [32]).

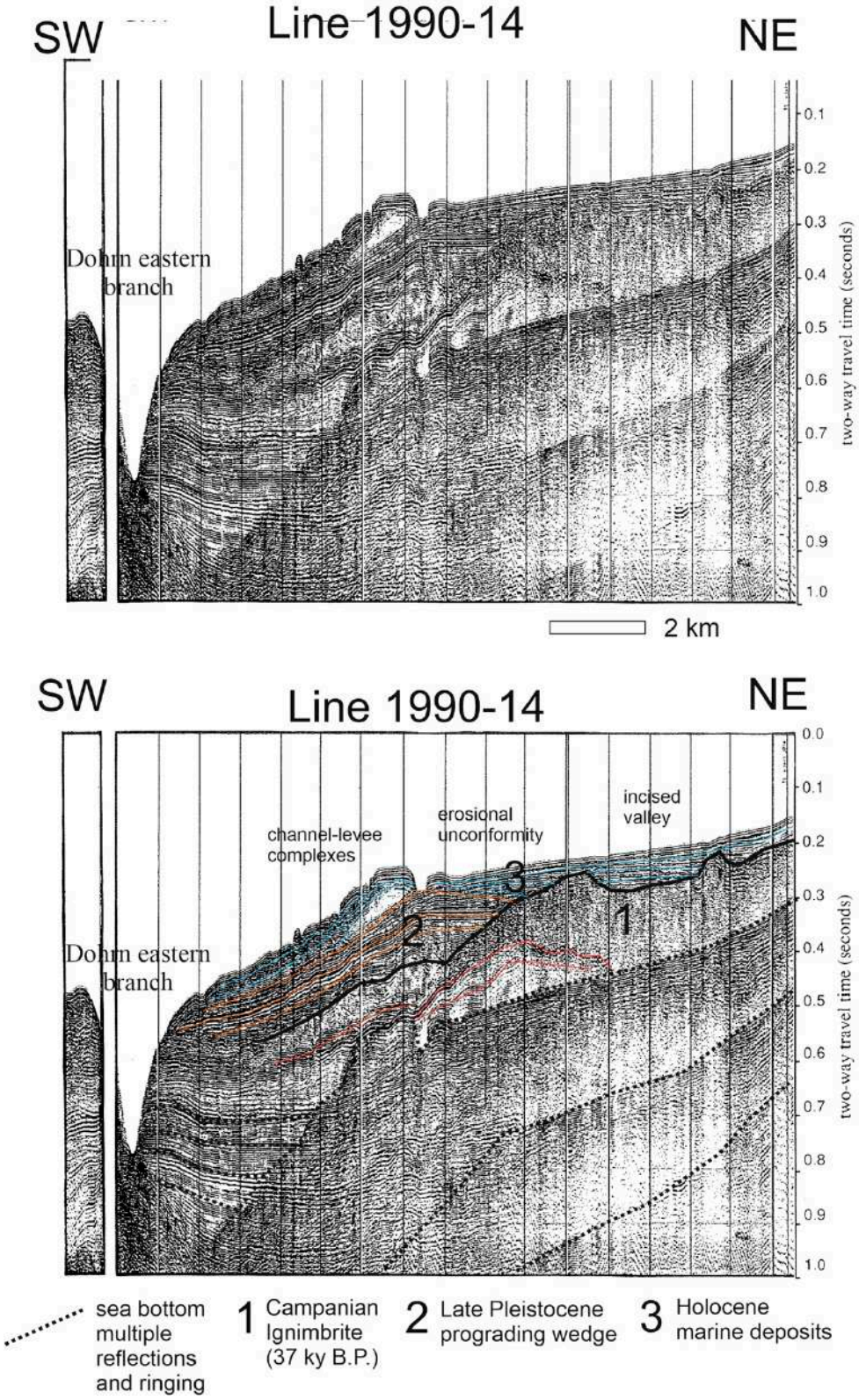


**Figure 13.** Seismic profile 1990-14 and corresponding geologic interpretation (modified after Fusi et al. [32]).

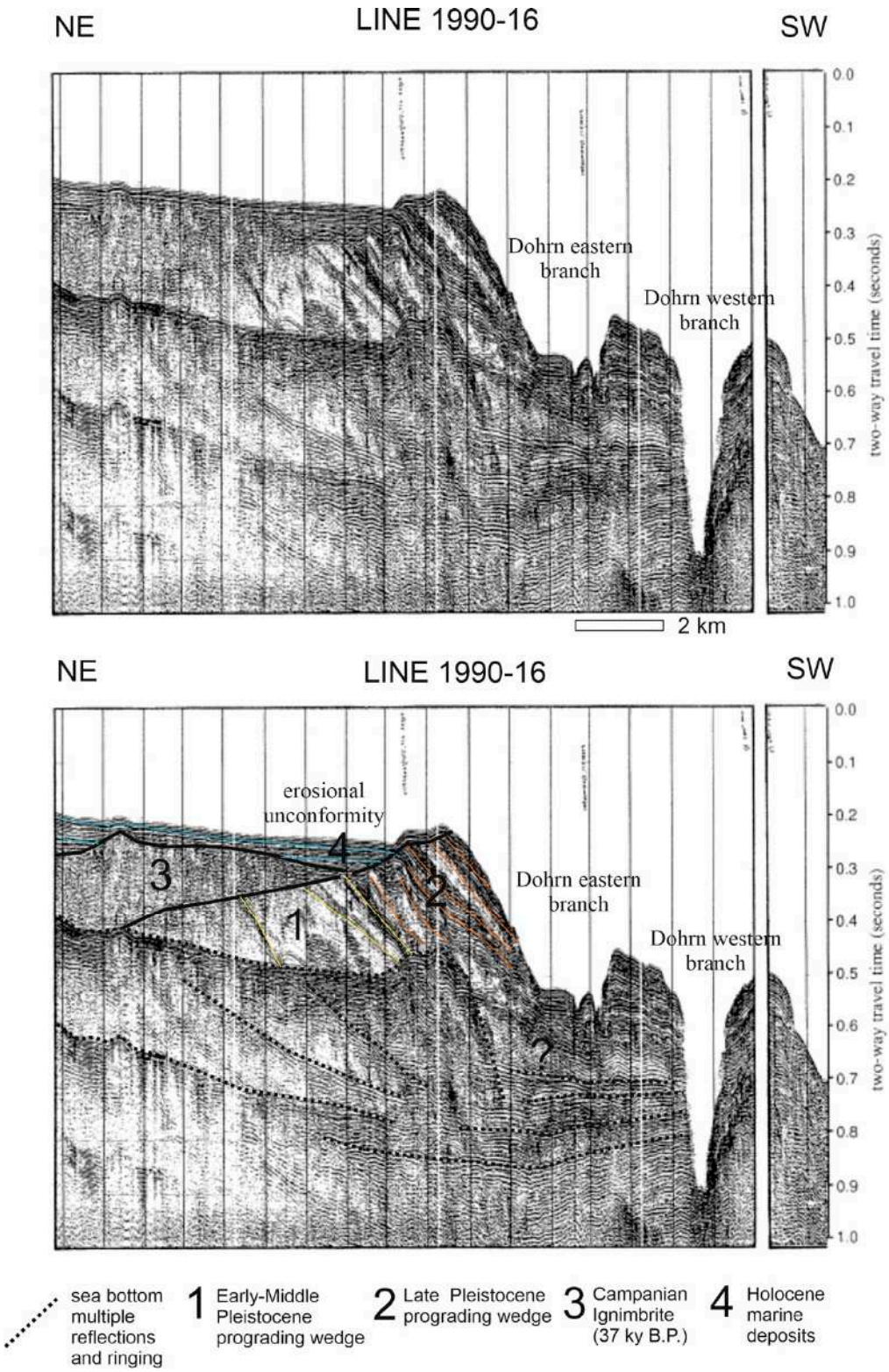


**Figure 14.** Seismic profile 1990-16 and corresponding geologic interpretation (modified after Fusi et al. [32]).

On the left in the seismic section, the volcanic unit of the Pentapalummo Bank is identified (Figure 11). The Pentapalummo Bank pertains to the submerged belt of the submarine banks located between Napoli and Pozzuoli. The corresponding seismic unit

(unit 6 in Figure 11) is characterized by mound-shaped geometry and by discontinuous seismic reflectors with a low amplitude (Figure 11).

Finally, unit 7 is interpreted as Holocene marine deposits, characterized by parallel and continuous seismic reflectors, thickening in correspondence with the central Bay of Naples, where this unit forms the stratigraphic bulk of the Ammontatura channel (Figure 11). The Ammontatura channel is an important channel of the Bay of Naples (Figure 4) and is genetically related to the western branch of the Dohrn canyon.

The stratigraphic architecture of the Bay of Naples in correspondence with the branches of the Dohrn canyon (both the western and the eastern one) is shown by the geological interpretation of seismic profile 1990-07 (Figure 12). Six seismic units are recognized based on the above listed seismo-stratigraphic criteria. Progradational reflectors, highly continuous, alternating with intervals of acoustically transparent seismic facies, are interpreted as the Early–Middle Pleistocene prograding wedge (unit 1 in Figure 12). This unit is overlain with onlap by seismic unit 2, characterized by continuous progradational bodies, less inclined than those of unit 1 and interpreted as a Middle Pleistocene transgressive sequence (see also Figure 11).

The geological interpretation shows that the Dohrn eastern branch is completely incised in the Late Pleistocene prograding wedge (unit 3 in Figure 12), characterized by continuous progradational reflectors, alternating with acoustically transparent intervals. In the south-eastern flank of the canyon, an important erosional unconformity truncates this prograding wedge in its upper part, as shown on the right side of Figure 12.

In the middle between the two branches of the canyons, a wide sedimentary body, characterized by discontinuous seismic reflectors and by a wedge shape (unit 4 in Figure 12), is interpreted as a submarine slide, showing the activity of gravitational processes on the Naples slope (Figure 12).

Unit 5 in Figure 12 is interpreted as the volcanic unit of the Pentapalummo Bank, characterized by discontinuous seismic reflectors and by mound-shaped geometry (Figure 12). The occurrence of this unit also shows that in this area the contribution of volcanism to the stratigraphic architecture is important.

The geological interpretation of seismic profile 1990-07 shows that the Dohrn western branch is incised in the sedimentary seismic units on its south-eastern flank and in the volcanic seismic units on the north-western one (Figure 12). This implies that the origin of this canyon is controlled by both sedimentary and volcanic processes (Figure 12).

A relict morphology of the Late Pleistocene prograding wedge is shown by the geological interpretation of seismic profile 1990-14 (Figure 13). This morphology is composed of the seismic reflectors of unit 2, interpreted as the Late Pleistocene prograding wedge (Figure 13; see also Figures 11 and 12).

A wide seismic unit, wedged-shaped, is characterized by an acoustically transparent seismic facies passing into a seismic facies with discontinuous seismic reflectors of high amplitude (unit 1 in Figure 13). This unit has been interpreted as the volcanic seismic unit of the Campanian Ignimbrite. The top of this seismic unit is distinguished from a regional unconformity, whose erosional nature is suggested by incised valleys (Figure 13).

A wide incised valley, located at the top of the CI seismic unit, may indicate a relative sea level fall, occurring during or after the individuation of this unconformity (Figure 13). Based on the inferred age of the CI seismic unit (37 ky B.P.), it can be assumed that the relative sea level fall is younger than 37 ky B.P. The incised valley is filled with parallel and continuous seismic reflectors, interpreted as the Holocene marine deposits (unit 3 in Figure 13). Unit 3 is also characterized by the possible occurrence of channel–levee complexes based on the observed seismic facies. In fact, an acoustically transparent body may be interpreted as a sandy levee, buried by Holocene deposits and suggesting the activity of geological processes of overbanking in the surroundings of the Naples canyons (Figure 13).

The geological interpretation of seismic profile 1990-16 shows the stratigraphic architecture of Naples Bay in correspondence with the Dohrn canyon, whose branches are clearly seen (Figure 14). Four seismic units are recognized based on the geological inter-

pretation. Seismic unit 1 is typified by prograding and continuous reflectors, alternating with acoustically transparent intervals, and is interpreted as the Early–Middle Pleistocene prograding wedge. This unit grades upwards, without an angular unconformity, into seismic unit 2, characterized by continuous seismic reflectors and interpreted as the Late Pleistocene prograding wedge. The vertical stacking of seismic units 1 and 2 gives rise to a relict morphology, located on the canyon's side (see also Figure 13). Unit 3 shows wedged-shaped external geometry and an acoustically transparent seismic facies. It is interpreted as the Campanian Ignimbrite (CI) seismic unit. The top of this unit consists of an important erosional unconformity, dipping landwards, involving the continental shelf areas (Figure 14). Seismic unit 4 shows parallel and continuous seismic reflectors and is interpreted as Holocene marine deposits.

A detailed seismic section of the multichannel seismic profile (NAM 3) was constructed, starting from the regional seismic profile that was previously published [35]. Three main regional unconformities are reported (A, B, C), separating five main seismo-stratigraphic units (1, 2, 3, 4/4a, and 5). While seismo-stratigraphic unit 1 corresponds with the Middle–Late Pleistocene transgressive sequence, seismo-stratigraphic units 2 and 3 correspond with the Late Pleistocene prograding wedge (Figures 11–14). An important regional unconformity (unconformity B) can be recognized in the inner part of the Late Pleistocene prograding wedge, fed by the Sarno River mouth (Figure S10). This unconformity is shown on the right side of Figure 12. Seismo-stratigraphic unit 4a, with wedge-shaped geometry, corresponds with the CI unit (Campanian Ignimbrite) [5,47–59]. Late Pleistocene progradations and Late Pleistocene slope sequences are also individuated (Figure S10).

A re-interpretation of seismic profile GRNA51 (Figure S11), recorded during the oceanographic cruise GMS00-05 and previously interpreted with the magnetic data of the Bay of Naples [95], was carried out. The proposed seismic line is a near trace line, processed through preliminary processing by applying a Butterworth bandpass filter and using the frequencies of 40 Hz, 45 Hz, 240 Hz, and 250 Hz. We constructed this detailed geological interpretation to show a seismic line crossing the depositional system of the Naples canyons (Figure S11), further constraining the stratigraphic architecture shown in Figures 11–14.

Two sub-bottom Chirp profiles were selected in order to show the stratigraphic architecture of the Bay of Naples (Figures S12 and S13). Figure S12 shows the morpho-structural lineament of the Pentapalummo Bank, characterized by volcanic acoustic basement. The north-eastern slope of this volcanic bank is distinguished from a sedimentary drape composed of Holocene deposits and by slope instability in correspondence with a slide scar. At the toe-of-slope, a seismo-stratigraphic unit, wedged-shaped and chaotic as seismic facies, is interpreted as debris flow deposits (Figure S12).

Figure S13 shows sub-bottom profile NA16_1 showing the Pentapalummo Bank and its south-western slope, characterized by the volcanic acoustic basement and by a thin drape of Holocene deposits. The recent sedimentary cover appears to be quite reduced compared with the north-eastern slope. At the toe-of-slope, a main tributary channel is identified: it appears to be filled by recent deposits and is bounded by a channel levee. This channel drains the volcaniclastic and sedimentary input of the Bay of Naples towards the continental slope.

## 5. Discussion

The sedimentary dynamics of the coastal areas of the Bay of Naples have been analyzed based on sedimentological, morpho-bathymetric, and seismo-stratigraphic data.

The geologic and morpho-bathymetric setting of the Naples canyons must be placed in the framework of the Mediterranean canyons. The Mediterranean canyons are closely spaced, dendritic, shorter, and deeper than the other canyons of the world [1]. During the Messinian salinity crisis of the Mediterranean Sea, the regional canyon's development was mainly controlled by the relative sea level fall and by desiccation. The Mediterranean continental margins have undergone subaerial exposure and erosion at a regional scale [17,95], triggering the subsequent formation of the submarine canyons. During the subaerial ex-

posure of the Mediterranean continental margins, incipient canyons developed due to the submarine erosion, which followed the re-filling of the Mediterranean Sea [1,17,95]. However, based on seismo-stratigraphic evidence of the data analyzed in this paper, it can be assessed that the Dohrn and Magnaghi canyons of Naples Bay formed during time intervals younger than the Late Miocene, and no direct relationships exist with the formation of canyons in the Mediterranean during the Late Miocene, which occurred mainly on the northern continental margins of the Mediterranean [1,96,97].

Important geological data on the Naples canyons have been highlighted in previous scientific literature. Milia [8] highlighted that the formation of the Dohrn canyon can be interpreted as the response to the eustatic fall and to the tectonic uplift of the outer shelf of Naples Bay. The geological interpretation of Sparker profiles shows that the Dohrn canyon carves the Middle Pleistocene deposits of Naples Bay. Based on the interpretation of this author, the canyon erodes the Early–Middle Pleistocene prograding wedge [8]. On the contrary, our seismo-stratigraphic data show that the Dohrn canyon erodes the Late Pleistocene deposits of the upper prograding wedge, composing the stratigraphic architecture of Naples Bay (Figures 11–14). Based on our seismo-stratigraphic interpretation, the formation of the Dohrn canyon is younger than that of both the Early–Middle Pleistocene prograding wedge and the Middle Pleistocene transgressive sequence (Figures 11–14). Based on previous geological interpretations, the eustatic sea level fell at a point corresponding to the mouth of a river located near the shelf edge. In our interpretation, we suggest that the formation of the Dohrn canyon was triggered by the increased volcaniclastic input in the Naples Bay during extensive ignimbrite eruption, including the Campanian Ignimbrite and the Neapolitan Yellow Tuff. Moreover, the Acerra–Dohrn canyon fault (Figure 1) may have played an important role as a tectonic control on the individuation of the canyon, being an important counter-Apenninic regional lineament controlling Naples Bay.

Aiello et al. [34] previously highlighted the occurrence of two non-volcanic bathymetric highs located next to the heads of the Dohrn canyon at the center of the bay based on Multibeam and Sparker interpretation. In this paper, we have described these structures in detail (Figures 13 and 14), showing that they are in stratigraphic relationship with the seismic unit genetically related to the Campanian Ignimbrite (37 ky B.P.) [5,47–59].

Previous analysis of morpho-bathymetric data showed that important submarine gravity instabilities exist in the Dohrn and Magnaghi canyons [38–40], as shown by core data integrated stratigraphy in the Dohrn submarine [31]. Di Fiore et al. [40] highlighted that the main morphological lineaments of the canyon system are represented by the canyon walls, the drainage axes, the slide scars, and the canyon axes. The morpho-bathymetric data of our analysis (Figures 4 and S1–S5) are in overall agreement with the data of Di Fiore et al. [40], adding further details to the morpho-bathymetric interpretation. Figures S1–S5 shows that both V-shaped and U-shaped erosional features are widespread in the Naples canyon system. Gamberi et al. [98] displayed regional morpho-bathymetric data on the southern Tyrrhenian Sea, including the interpretation of the bathymetry of the Campania–Latium margin. A "tortuous corridor" was interpreted in the Latium–Campanian slope, individuated by normal faults parallel to the continental margin. The tectonic structures are important controlling factors in producing the extent of dip and strike sectors and in controlling the depositional and the erosional areas of submarine canyons and gullies [98]. The data analyzed in this paper are in agreement with the tectonic interpretation of Gamberi et al. [98], as we have suggested the important role of the Acerra–Dohrn fault (Figure 1) in controlling the stratigraphic architecture of Naples Bay and of the Dohrn canyon.

In discussing the morpho-bathymetric data analyzed in this paper, we have applied to the Naples canyons the model of Pratson and Coakley [9]. This model simulates a three-stage sequence for the formation of the submarine canyons and the following in particular:

(1) The erosion of the pre-canyon channels, which starts in peculiar sites of the upper slope, where the slope gradient exceeds critical values due to the high rates of sedimentation;

(2) The localized failures of the slope on the walls and on the bottom of the pre-canyon channels, in one or more sites of the intermediate and lower slope, triggered by the erosion of sediment fluxes;
(3) The evolution of the slope failures in a canyon with a retreating head, advancing upwards on the slope along the pre-canyon channels, due to the retrogressive slides induced by sediment fluxes.

The DEM of Naples Bay (Figure 4) shows that the Dohrn canyon represents the most important morphological structure of the bay and develops along two branches, joining in a main valley, which is relatively flat and has amplitudes ranging between 200 m and 1 km. The canyon slopes are relatively steep, often terraced (Figure S2), and are often characterized by slide scars (Figure S12). On the southeastern flank of the canyon system, four linear incisions, which are parallel, suggest a structural control from ENE–SWS trending faults (Figure 4). Both the Magnaghi canyon and the western branch of the Dohrn canyon show hints of retreating canyon heads. In particular, the Magnaghi canyon shows a triple retrogressive head, while the Dohrn western branch shows a double regressive head (Figure 4).

Accordingly to this model, the regressive heads of the Naples canyons evolved from retrogressive submarine slides, which were induced by intense sediment fluxes, in this case volcaniclastic, and were controlled by the considerable ignimbrite eruptions of the Campanian Ignimbrite and of the Neapolitan Yellow Tuff. This interpretation is confirmed by seismo-stratigraphic evidence (Figures 11–14). The retrogressive submarine slides are located in the surroundings of the present-day heads but also in the lower part of the branches (Figure 4).

The seismo-stratigraphic data analyzed in this paper (Figures 11–14, S10 and S11) show that a close linkage exists between the Naples canyons and the ignimbrite eruptions of the Campania Plain, in particular the Campanian Ignimbrite (CI; 37 ky B.P.) [47–59] and the Neapolitan Yellow Tuff (NYT; 19 ky B.P.) [60–65].

The Campi Flegrei volcanism is divided based on two main volcanic events, whose deposits represent important stratigraphic markers in the whole volcanic district. The first of two events gave rise to the emplacement of the Campania Grey Tuff (or Campanian Ignimbrite *Auct.*), around 39 ky B.P. ($^{40}Ar/^{39}Ar$). The second one is the eruption of the Neapolitan Yellow Tuff, dated to 15 ky B.P. [6]. Both volcanic eruptions contributed to the formation of collapsed caldera structures, which are dominant structures of the whole volcanic district [51,53,56].

Campi Flegrei is an active volcanic field, also including the western sector of Naples town. Many authors agree in considering the Gulf of Pozzuoli and the surrounding area as the result of a set of successive caldera downthrows [51,53,56]. In particular, Rosi and Sbrana [51] showed that the stratigraphic succession Piperno-Breccia Museo represents the proximal facies of the Campanian Ignimbrite, welded and coarse-grained and outcropping at the caldera rim. Scandone et al. [52] interpreted the caldera rim as produced by a younger eruption, i.e., the Neapolitan Yellow Tuff, which occurred at 15 ky B.P. [6]. Barberi et al. [47] suggested three calderas, with the inner one as the youngest; these calderas were suggested to be associated with the Campanian Ignimbrite and the yellow tuffs of the younger eruptive centers. The caldera rim of the Neapolitan Yellow Tuff has been recognized in outcrop only along the northern slope of the Posillipo hill (Naples town),while other parts are buried below the products of the younger Phlegrean volcanic activity [60]. The eastern rim of the caldera associated with the Campanian Ignimbrite was widened eastwards by Orsi et al. [53], including most of Naples town. The geological survey of the proximal succession of the Campanian Ignimbrite (Piperno-Breccia Museo) in Naples town detailed the trending of this volcano –tectonic structure in the urban area of Naples [56]. Sacchi et al. [62] showed the stratal architecture and the kinematic reconstruction of the Neapolitan Yellow Tuff caldera offshore the Campi Flegrei volcanic complex based on seismo-stratigraphic data.

The relationships between the ignimbrite eruptions and the regional faults in the Campania region were highlighted by Torrente et al. [99], who recognized a spatial and a temporal link between volcanism and tectonics. In particular, a fissure eruptive mechanism was recognized, as the sources of the ignimbrites were aligned with the regional faults. Moreover, thick ignimbrite wedged-shaped successions filling the half-graben structures suggest that the activity of the normal faults and the ignimbrite are contemporaneous. The ignimbrite eruptive centers, consisting of the pre-Campania Ignimbrite tuffs (290 ky B.P.) and of the Campanian Ignimbrite (39 ky B.P.), are widespread in the whole Campania region but were concentrated at the Campi Flegrei during the NYT eruption [99].

The seismo-stratigraphic data analyzed in this paper (Figures 11–14) show that thick ignimbrite wedges occur in Naples Bay, as wedge-shaped, acoustically transparent seismic units, in agreement with the data from previous papers [99], detecting these volcano–tectonic structures onshore, filling half-graben basins.

The seismo-stratigraphic architecture of the Campania continental margin is herein shown based on Sparker data interpretation, reassessed after Fusi et al. [32] (Figures 11–14) and after D'Argenio et al. [35] (Figure S10). The filling of the half-graben of Naples Bay consists of two prograding wedges, each one characterized by a distinct acoustic pattern and seismic facies. The first wedge is characterized by alternating intervals of continuous and parallel seismic reflectors and of acoustically transparent intervals. This progradational unit, dipping north-west, shows eroded topsets and preserved clinoforms and has been interpreted as a relict prograding wedge, probably Early–Middle Pleistocene in age, having its depocenter between the Sorrento Peninsula and the Capri Island. On the continental shelf (Figure 12) the seismic reflectors are truncated by an erosional unconformity, probably subaerial, indicating a relative sea level fall and a seaward shifting of coastal and marine facies, together with a sedimentary bypass and strong erosion of the shelf and upper slope. A transgressive unit is interposed between the two prograding wedges (Figures 11–14 and S10), deposited during the sea level rise that followed the sea level fall corresponding to the subaerial unconformity on which the shelf truncates the seismic reflectors of the first prograding wedge (Figure 12). The second prograding wedge overlies the transgressive unit and is characterized by continuous seismic reflectors, with a sigmoidal pattern. The progradation of the upper wedge happens from SE to NW, showing entry points of the wedge coming from the Capri-Sorrento structural high. Proceeding basinwards, the seismic reflectors of the upper wedge tend to become sub-parallel. This unit gives rise to relict morphologies (Figures 13 and 14), located in correspondence with the present-day shelf break and the eastern branch of the Dohrn canyon (Figure 4).

## 6. Conclusions

Three main areas have been distinguished based on the sedimentological data analysis, i.e., the continental shelf of Naples Bay, the Phlegrean banks (Pentapalummo, Nisida, and Miseno), and the Naples canyons (Dohrn and Magnaghi), having different facies characteristics.

The Phlegrean banks are characterized by a sandy facies, where the bioclastic component is significant. This facies can be interpreted as the "detritique cotier" *sensu* Peres and Picard [100]. Below the limit of the infralittoral stage, the circalittoral stage begins with some current or recent debris formations, called "detritique cotier", whose nature is variable. These debris formations include several facies, such as the facies a pralines, the facies with *Haranacnion Spatulatum*, the facies with *Ophiura texturata*, the facies a mäerl, and the facies with several species of *Lithothamnium* (rhodalgal facies) [100].

In Naples Bay, the rhodalgal facies is widespread on the Phlegrean banks, where it is controlled by the location of the platform, by the morpho-bathymetric structure, and by the hydrodynamic factors. The top of the banks is located at water depths ranging between 20 m and 30 m (Figures S12 and S13), where *Posidonia Oceanica* meadows are also widespread.

The sedimentological data show that the continental shelf of Naples Bay is characterized by a sandy facies, composed of sandy silts and silty sands, typical of mixed carbonate siliciclastic systems. This facies is widespread on both the Tyrrhenian and Adriatic conti-

nental margins. On the Tyrrhenian continental margin, sedimentary facies and the mixing of heterozoan and siliciclastic sediments in temperate waters on the continental shelf of the Pontian Archipelago have been described in detail [101]. In the Bay of Naples, mixed carbonate–siliciclastic systems have recently been described [102].

The core lithostratigraphic data show the importance of the tephra levels in Naples Bay, interstratified in the Quaternary marine deposits (Figures 8–10). One of the most important tephra in the Naples Bay is the 79 D.C. tephra, but significant tephra deposits have also been recognized in the Ammontatura Channel, which is genetically related to the Dohrn canyon, and in the canyon itself [31]. Seismo-stratigraphic evidence showing Late Pleistocene relict morphologies located at the center of the bay and located in correspondence of the present-day Dohrn eastern branch [31] (Figure 13) suggests that the Dohrn canyon belongs to the second category of Buhrig et al. [14].

The development of the Dohrn canyon is controlled by fluvial processes, active in correspondence with the palaeo-Schiazzano River system, and by the main eruptive events involving the submarine portion of Naples Bay, including the Campanian Ignimbrite (CI; 39 ky B.P.) and the Neapolitan Yellow Tuff (NYT; 15 ky B.P.). The regional counter-apenninic faults, and in particular the Acerra–Dohrn fault (Figure 1), have played a major role in controlling both the stratigraphic architecture of Naples Bay and the Dohrn canyon formation. The Magnaghi canyon is controlled by the erosional processes on the continental slope of Procida Island, which were active during the last eruptive phases of the island (Solchiaro Formation; 18 ky B.P.), triggering high rates of volcaniclastic supply.

Based on the model of Pratson and Coakley [9] and taking into account seismo-stratigraphic evidence, the erosion of the pre-canyon channels (first stage of the Pratson and Coakley model) took place during a time interval ranging between the eruption of the Campanian Ignimbrite (CI; 37 ky B.P.) and the eruption of the Neapolitan Yellow Tuff (NYT; 15 ky B.P.).

The individuation of the canyon through localized failures on the slope (second stage of the Pratson and Coakley model) was younger than 15 ky B.P. (NYT eruption), while the abrupt termination of the Dohrn western branch towards the Nisida Bank led us to assume that the third stage (formation of retrogressive heads) is pre-dated by the emplacement of the Nisida Bank and of the Nisida volcanic complex.

The third phase of the canyon evolution is quite recent.

Steinmann et al. [103] showed a previously unknown seismic unit (V2), occurring between Nisida Island and the Nisida Bank, and interpreted as a previously unidentified volcanic mound, whose inferred age is <5 ka. Seismic unit V2 was probably formed during the Volcanic Epoch III between 4.8 and 3.8 ka [103].

**Supplementary Materials:** The following supporting information can be downloaded at: https://www.mdpi.com/article/10.3390/geosciences13080226/s1.

**Author Contributions:** Conceptualization, G.A. and M.C.; methodology, G.A.; software, M.C.; formal analysis, G.A.; investigation, G.A. and M.C.; data curation, M.C.; writing—original draft preparation, G.A.; writing—review and editing, G.A. All authors have read and agreed to the published version of the manuscript.

**Funding:** This research received no external funding.

**Data Availability Statement:** Not applicable.

**Conflicts of Interest:** The authors declare no conflict of interest.

## References

1. Harris, P.T.; Whiteway, T. Global distribution of large submarine canyons. Geomorphic differences between active and passive continental margins. *Mar. Geol.* **2011**, *285*, 69–86. [CrossRef]
2. Harris, P.T.; McMillan Lawler, M.; Rupp, J.; Baker, E.K. Geomorphology of the oceans. *Mar. Geol.* **2014**, *352*, 4–24. [CrossRef]
3. Harris, P.T.; McMillan Lawler, M. Geomorphology of Mediterranean submarine canyons in a global context—Results from a multivariate analysis of canyon geomorphic statistics. In *Submarine Canyon Dynamics in the Mediterranean and Tributary Seas—An Integrated Geological, Oceanographic and Biological Perspective*, 1st ed.; Briand, F., Ed.; CIESM Publisher: Monaco, Monaco, 2015; Volume 47, pp. 23–25.

4. Fildani, A. Submarine canyons: A brief review looking forward. *Geology* **2017**, *45*, 383–384. [CrossRef]
5. Di Vito, M.A.; Isaia, R.; Orsi, G.; Southon, J.; De Vita, S.; D'Antonio, M.; Pappalardo, L.; Piochi, M. Volcanic and deformational history of the Campi Flegrei caldera in the past 12 ka. *J. Volcanol. Geotherm. Res.* **1999**, *91*, 221–246. [CrossRef]
6. Deino, A.L.; Orsi, G.; De Vita, S.; Piochi, M. The age of the Neapolitan Yellow Tuff caldera-forming eruption (Campi Flegrei caldera, Italy) assessed by $^{40}Ar/^{39}Ar$ dating method. *J. Volcanol. Geotherm. Res.* **2004**, *133*, 157–170. [CrossRef]
7. Aiello, G.; Insinga, D.; Iorio, M.; Meo, A.; Senatore, M.R. On the occurrence of the Neapolitan Yellow Tuff tephra in the Northern Phlegraean Fields offshore (Eastern Tyrrhenian margin; Italy). *Ital. J. Geosci.* **2017**, *136*, 263–274. [CrossRef]
8. Milia, A. The Dohrn canyon: A response to the eustatic fall and tectonic uplift of the outer shelf along the eastern Tyrrhenian sea margin, Italy. *Geo-Mar. Lett.* **2000**, *20*, 101–108. [CrossRef]
9. Pratson, L.F.; Coakley, B.J. A model for the headward erosion of submarine canyons induced by downslope-eroding sediment flows. *Geol. Soc. Am. Bull.* **1996**, *108*, 225–234. [CrossRef]
10. Pratson, L.F.; Nittrouer, C.A.; Wilberg, P.L.; Steckler, M.S.; Swenson, J.B.; Cacchione, D.A.; Karson, J.A.; Murray, A.B.; Wolinsky, M.A.; Gerber, T.P.; et al. Seascape evolution on clastic continental shelves and slopes. In *Continental Margin Sedimentation: From Sediment Transport to Sequence Stratigraphy*, 1st ed.; Nittrouer, C.A., Austin, J.A., Field, M.E., Kravitz, J.H., Syvitski, J.P.M., Wilberg, P.L., Eds.; Wiley: New York, NY, USA, 2007; pp. 339–380.
11. Puig, P.; Palanques, A.; Martin, J. Contemporary sediment-transport processes in submarine canyons. *Annu. Rev. Mar. Sci.* **2014**, *6*, 53–77. [CrossRef]
12. Amblas, D.; Ceramicola, S.; Gerber, T.P.; Canals, M.; Chiocci, F.L.; Dowdeswell, J.A.; Harris, P.T.; Huvenne, V.A.I.; Lai, S.Y.J.; Lastras, G.; et al. Submarine canyons and gullies. In *Submarine Geomorphology*, 1st ed.; Micallef, A., Krastel, S., Savini, A., Eds.; Springer: Berlin/Heidelberg, Germany, 2017; pp. 251–272.
13. Matos, F.L.; Ross, S.W.; Huvenne, V.A.I.; Davies, J.S.; Cunha, M.R. Canyons pride and prejudice: Exploring the submarine canyon research landscape, a history of geographic and thematic bias. *Prog. Oceanogr.* **2018**, *169*, 6–19. [CrossRef]
14. Bührig, L.H.; Colombera, L.; Patacci, M.; Mountney, N.P.; McCaffrey, W.D. A global analysis of controls on submarine-canyon geomorphology. *Earth Sci. Rev.* **2022**, *233*, 104150. [CrossRef]
15. Li, S.; Alves, T.M.; Li, W.; Wang, X.; Rebesco, M.; Li, J.; Zhao, F.; Yu, K.; Wu, S. Morphology and evolution of submarine canyons on the northwest South China Sea margin. *Mar. Geol.* **2022**, *443*, 106695. [CrossRef]
16. Chiocci, F.L.; Orlando, L.; Tortora, P. Small-scale seismic stratigraphy and paleogeographical evolution of the continental shelf facing the SE Elba island (Northern Tyrrhenian Sea, Italy). *J. Sediment. Res.* **1991**, *61*, 506–526.
17. Druckman, Y.; Buchbinder, B.; Martinotti, G.M.; Siman Tov, R.; Aharon, P. The buried Afiq canyon (eastern Mediterranean, Israel): A case study of a Tertiary submarine canyon exposed in Late Messinian times. *Mar. Geol.* **1995**, *123*, 167–185. [CrossRef]
18. De Pippo, T.; Ilardi, M.; Pennetta, M. Main observations on genesis and morphological evolution of submarine valleys. *Zeitsch Fur Geomorphol.* **1999**, *43*, 91–111. [CrossRef]
19. Hernandez-Molina, F.; Somoza, L.; Lobo, F. Seismic stratigraphy of the Gulf of Cadiz continental shelf. A model for Late Quaternary very high resolution sequence stratigraphy and response to sea level fall. In *Sedimentary Responses to Forced Regressions*; Geological Society of London: London, UK, 2000; Volume 172, pp. 329–362.
20. Lericolais, G.; Auffret, M.; Bourillet, J.F. The Quaternary Channel River: Seismic stratigraphy of its palaeo-valleys and deeps. *J. Quat. Sci.* **2003**, *18*, 245–260. [CrossRef]
21. Bourillet, F.; Zaragosi, S.; Mulder, T. The French Atlantic margin and deep sea submarine systems. *Geo-Mar. Lett.* **2006**, *26*, 311–315. [CrossRef]
22. Gupta, S.; Collier, J.S.; Felgate, A.P.; Potter, G. Catastrophic flooding origin of shelf valley systems in the English Channel. *Nature* **2007**, *448*, 342–345. [CrossRef]
23. Toucanne, S.; Zaragosi, S.; Bourillet, J.F.; Marieu, V.; Cremer, M.; Kageyama, M.; Van Vliet Lanoe, B.; Eynaud, F.; Turon, J.L.; Gibbard, P.L. The first estimation of Fleuve Manche palaeoriver discharge during the last deglaciation: Evidence for Fennoscandian ice sheet meltwater flow in the English Channel ca 20–18 ka ago. *Earth Planet. Sci. Lett.* **2010**, *290*, 459–473. [CrossRef]
24. Molisso, F.; Caccavale, M.; Capodanno, M.; Di Gregorio, C.; Gilardi, M.; Guarino, A.; Oliveri, E.; Tamburrino, S.; Sacchi, M. Sedimentological analysis of marine deposits off the Bagnoli-Coroglio Site of National Interest (SNI), Pozzuoli (Napoli) Bay. *Chem. Ecol.* **2020**, *36*, 565–578. [CrossRef]
25. Sacchi, M.; Caccavale, M.; Corradino, M.; Esposito, G.; Ferranti, L.; Hamori, Z.; Horvath, F.; Insinga, D.; Marino, C.; Matano, F.; et al. The use and beauty of ultra-high resolution seismic reflection imaging in late quaternary volcaniclastic settings, bay of Naples, Italy/Ultra nagy felbontású reflexiós szeizmikus képalkotás haszna és szépségei: Késo-negyedidoszaki tengeri vulkanoklasztos felépítménvek a Nápolvi-Obölben. *Foldt. Kozlony* **2019**, *149*, 371–394.
26. Puig, P.; Duran, R.; Munoz, A.; Elvira, E.; Guill'en, J. Submarine canyon-head morphologies and inferred sediment transport processes in the Alías-Almanzora canyon system (SW Mediterranean): On the role of the sediment supply. *Mar. Geol.* **2017**, *393*, 21–34. [CrossRef]
27. Lisiecki, L.E.; Raymo, M.E. A Pliocene-Pleistocene stack of 57 globally distributed benthic $\delta^{18}O$ records. *Paleoceanography* **2005**, *20*, PA1003. [CrossRef]
28. Rohling, E.J.; Braun, K.; Grant, K.; Kucera, M.; Roberts, A.P.; Siddall, M.; Trommer, G. Comparison between Holocene and Marine Isotope Stage-11 sea-level histories. *Earth Planet. Sci. Lett.* **2010**, *291*, 97–105. [CrossRef]
29. Dutton, A.; Lambeck, K. Ice Volume and Sea Level During the Last Interglacial. *Science* **2012**, *337*, 216. [CrossRef] [PubMed]

30. Stocchi, P.; Vacchi, M.; Lorscheid, T.; de Boer, B.; Simms, A.R.; van de Wal, R.S.W.; Vermeersen, B.L.A.; Pappalardo, M.; Rovere, A. MIS 5e relative sea-level changes in the Mediterranean Sea: Contribution of isostatic disequilibrium. *Quat. Sci. Rev.* **2018**, *185*, 122–134. [CrossRef]
31. Aiello, G.; Iorio, M.; Molisso, F.; Sacchi, M. Integrated Morpho-Bathymetric, Seismic-Stratigraphic, and Sedimentological Data on the Dohrn canyon (Naples Bay, Southern Tyrrhenian Sea): Relationships with Volcanism and Tectonics. *Geosciences* **2020**, *10*, 319. [CrossRef]
32. Fusi, N.; Mirabile, L.; Camerlenghi, A.; Ranieri, G. Marine geophysical survey of the Gulf of Naples (Italy): Relationship between submarine volcanic activity and sedimentation. *Mem. Soc. Geol. Ital.* **1991**, *47*, 95–114.
33. Mirabile, L.; De Marinis, E.; Frattini, M. The Phlegrean Fields beneath the sea: The underwater volcanic district of Naples, Italy. *Boll. Geof. Teor. Appl.* **2000**, *41*, 159–186.
34. Aiello, G.; Budillon, F.; Cristofalo, G.; D'Argenio, B.; De Alteriis, G.; De Lauro, M.; Ferraro, L.; Marsella, E.; Pelosi, N.; Sacchi, M.; et al. Marine Geology and Morphobathymetry in the Bay of Naples (South-Eastern Tyrrhenian Sea, Italy). In *Mediterranean Ecosystems*, 1st ed.; Faranda, F.M., Guglielmo, L., Spezie, G., Eds.; Springer: Milano, Italy, 2001; pp. 1–8.
35. D'Argenio, B.; Aiello, G.; de Alteriis, G.; Milia, A.; Sacchi, M.; Tonielli, R.; Budillon, F.; Chiocci, F.L.; Conforti, A.; De Lauro, M.; et al. Digital Elevation Model of the Naples Bay and surrounding areas, Eastern Tyrrhenian sea, Italy. In *Mapping Geology in Italy*; Pasquarè, C., Venturini, C., Groppelli, G., Eds.; SELCA: Firenze, Italy, 2004; pp. 3–10.
36. Passaro, S.; Tamburrino, S.; Vallefuoco, M.; Tassi, F.; Vaselli, O.; Giannini, L.; Chiodini, G.; Caliro, S.; Sacchi, M.; Rizzo, A.; et al. Seafloor doming driven by degassing processes unveils sprouting volcanism in coastal areas. *Sci. Rep.* **2016**, *6*, 22448. [CrossRef]
37. Ruggieri, S.; Aiello, G.; Marsella, E. Integrated marine geophysical data interpretation of the Naples Bay continental slope (southern Tyrrhenian sea, Italy). *Boll. Geof. Teor. Appl.* **2007**, *48*, 1–24.
38. Aiello, G.; Marsella, E.; D'Isanto, C. Sistemi deposizionali di ambiente marino profondo ed instabilità gravitative sottomarine: Esempi di studio sulla scarpata sottomarina della Campania in base all'interpretazione integrata di dati di geofisica marina. *Atti Associaz. Ital. Oceanol. E Limnol.* **2008**, *19*, 9–20.
39. Aiello, G.; Marsella, E.; Passaro, S. Submarine instability processes on the continental slopes off the Campania region (Southern Tyrrhenian sea, Italy): The case history of Ischia island (Naples Bay). *Boll. Geof. Teor. Appl.* **2009**, *50*, 193–207.
40. Di Fiore, V.; Aiello, G.; D'Argenio, B. Gravity instabilities in the Dohrn Canyon (Bay of Naples, Southern Tyrrhenian Sea): Potential wave and run-up (tsunami) reconstruction from a fossil submarine landslide. *Geol. Carpathica* **2011**, *62*, 55–63. [CrossRef]
41. Locardi, E. Individuazione delle strutture sismogenetiche dall'esame dell'evoluzione vulcano-tettonica dell'Appennino e del Tirreno. *Mem. Soc. Geol. Ital.* **1982**, *24*, 569–596.
42. Ferranti, L.; Oldow, J.S. Pre-Quaternary orogen-parallel extension in the Southern Apennine belt, Italy. *Tectonophysics* **1996**, *260*, 325–347. [CrossRef]
43. Corrado, S.; Di Bucci, D.; Leschiutta, I.; Naso, G.; Trigari, A. La tettonica quaternaria della Piana d'Isernia nell'evoluzione strutturale del settore molisano. *Il Quat.* **1997**, *10*, 609–614.
44. Bruno, P.P.G.; Rapolla, A.; Di Fiore, V. Structural setting of the Bay of Naples (Italy) through seismic reflection data: Implications for Campanian volcanism. *Tectonophysics* **2003**, *372*, 193–213. [CrossRef]
45. Amoruso, A.; Crescentini, L.; Scarpa, R. Faulting geometry of the complex 1980 Campania-Lucania earthquake from leveling data. *Geophys. J. Int.* **2005**, *162*, 156–168. [CrossRef]
46. Milano, G.; Di Giovanbattista, R.; Ventura, G. Seismic activity in the transition zone between Southern and Central Apennines (Italy): Evidence of longitudinal extension inside the Ortona-Roccamonfina tectonic line. *Tectonophysics* **2008**, *457*, 102–110. [CrossRef]
47. Barberi, F.; Cassano, E.; La Torre, P.; Sbrana, A. Structural evolution of Campi Flegrei caldera in light of volcanological and geophysical data. *J. Volcanol. Geotherm. Res.* **1991**, *48*, 33–49. [CrossRef]
48. Cosentino, D.; De Rita, D.; Funiciello, R.; Parotto, M.; Salvini, F.; Vittori, E. Fracture System in Phlegrean Fields (Naples, Southern Italy). *Bull. Volcanol.* **1984**, *47*, 247–257. [CrossRef]
49. Di Girolamo, P.; Ghiara, M.R.; Lirer, L.; Munno, R.; Rolandi, G.; Stanzione, D. Vulcanologia e petrologia dei Campi Flegrei. *Boll. Soc. Geol. Ital.* **1984**, *103*, 349–413.
50. Cinque, A.; Rolandi, G.; Zamparelli, V. L'estensione dei depositi marini olocenici nei Campi Flegrei in relazione alla vulcanotettonica. *Boll. Soc. Geol. Ital.* **1985**, *104*, 327–348.
51. Rosi, M.; Sbrana, A. Phlegrean Fields. In *Quaderni de La Ricerca Scientifica*; CNR: Rome, Italy, 1987.
52. Scandone, R.; Bellucci, F.; Lirer, L.; Rolandi, G. The structure of the Campanian Plain and the activity of the Neapolitan volcanoes. *J. Volcanol. Geotherm. Res.* **1991**, *48*, 1–31. [CrossRef]
53. Orsi, G.; De Vita, S.; Di Vito, M.A. The restless, resurgent Campi Flegrei nested caldera (Italy): Constraints on its evolution and its configuration. *J. Volcanol. Geotherm. Res.* **1996**, *74*, 179–214. [CrossRef]
54. Acocella, V.; Funiciello, R.; Marotta, E.; Orsi, G.; De Vita, S. The role of extensional structures on experimental calderas and resurgence. *J. Volcanol. Geotherm. Res.* **2004**, *129*, 199–217. [CrossRef]
55. Marianelli, P.; Sbrana, A.; Proto, M. Magma chamber of the Campi Flegrei supervolcano at the time of eruption of the Campanian Ignimbrite. *Geology* **2006**, *34*, 937–940. [CrossRef]

56. Perrotta, A.; Scarpati, C.; Luongo, G.; Morra, V. The Campi Flegrei caldera boundary in the city of Naples. In *Volcanism in the Campania Plain: Vesuvius, Campi Flegrei and Ignimbrites*, 1st ed.; De Vivo, B., Ed.; Elsevier Science Publishers: Amsterdam, The Netherlands, 2006; pp. 85–96.
57. Pyle, D.M.; Rickett, G.D.; Margari, V.; van Andel, T.H.; Sinitsyn, A.A.; Praslov, N.D.; Lisitsyn, S. Wide dispersal and deposition of distal tephra during the Pleistocene 'Campanian Ignimbrite/Y5' eruption, Italy. *Quat. Sci. Rev.* **2006**, *25*, 2713–2728. [CrossRef]
58. Fedele, F.; Giaccio, B.; Hajdas, I. Timescales and cultural process at 40,000 BP in the light of the Campanian Ignimbrite eruption, Western Eurasia. *J. Hum. Evol.* **2008**, *55*, 834–857. [CrossRef]
59. Giaccio, B.; Isaia, R.; Fedele, F.G.; Di Canzio, E.; Hoffecker, J.; Ronchitelli, A.; Sinitsyn, A.A.; Anikovich, M.; Lisitsyn, S.; Popov, V.V. The Campanian Ignimbrite and Codola tephra layers: Two temporal/stratigraphic markers for the Early Upper Palaeolithic in southern Italy and eastern Europe. *J. Volcanol. Geotherm. Res.* **2008**, *177*, 208–226. [CrossRef]
60. Scarpati, C.; Perrotta, A.; Cole, P.D. The Neapolitan Yellow Tuff—A large volume multiphase eruption from Campi Flegrei, Southern Italy. *Bull. Volcanol.* **1993**, *55*, 343–356. [CrossRef]
61. Pappalardo, L.; Civetta, L.; D'Antonio, M.; Deino, A.; Di Vito, M.A.; Orsi, G.; Carandente, A.; De Vita, S.; Isaia, R.; Piochi, M. Chemical and Sr-isotopical evolution of the Phlegraean magmatic system before the Campanian Ignimbrite and the Neapolitan Yellow Tuff eruptions. *J. Volcanol. Geotherm. Res.* **1999**, *91*, 141–166. [CrossRef]
62. Sacchi, M.; Pepe, F.; Corradino, M.; Insinga, D.D.; Molisso, F.; Lubritto, C. The Neapolitan Yellow Tuff caldera offshore the Campi Flegrei: Stratalarchitecture and kinematic reconstruction during the last 15 ky. *Mar. Geol.* **2014**, *354*, 15–33. [CrossRef]
63. Forni, F.; Petricca, E.; Bachmann, O.; Mollo, S.; De Astis, G.; Piochi, M. The role of magma mixing/mingling and cumulate melting in the Neapolitan Yellow Tuff caldera-forming eruption (Campi Flegrei, Southern Italy). *Contrib. Mineral. Petrol.* **2018**, *173*, 45. [CrossRef]
64. Rolandi, G.; Di Lascio, M.; Rolandi, R. The Neapolitan Yellow Tuff eruption as the source of the Campi Flegrei caldera. In *Vesuvius, Campi Flegrei, and Campanian Volcanism*, 1st ed.; De Vivo, B., Belkin, H.E., Rolandi, G., Eds.; Elsevier Science Publishers: Amsterdam, The Netherlands, 2020; pp. 273–296.
65. Corradino, M.; Pepe, F.; Sacchi, M.; Solaro, G.; Duarte, H.; Ferranti, L.; Zinno, I. Resurgent uplift at large calderas and relationship to caldera-forming faults and the magma reservoir: New insights from the Neapolitan Yellow Tuff caldera (Italy). *J. Volcanol. Geotherm. Res.* **2021**, *411*, 107183. [CrossRef]
66. Mariani, M.; Prato, R. Neogenic coastal basins of Tyrrhenian margin: Seismo-stratigraphic approach. *Mem. Soc. Geol. Ital.* **1988**, *41*, 519–531.
67. Brancaccio, L.; Cinque, A.; Romano, P.; Rosskopf, C.; Russo, F.; Santangelo, N.; Sgrosso, I. Geomorphology and neotectonic evolution of a sector of the Tyrrhenian flank of the southern Apennines (region of Naples, Italy). *Zeitsch Fur Geomorphol.* **1991**, *82*, 47–58.
68. Barra, D.; Romano, P.; Santo, A.; Campaiola, L.; Roca, V.; Tuniz, C. The Versilian transgression in the Volturno river plain (Campania, southern Italy): Palaeoenvironmental history and geochronological data. *Il Quat.* **1996**, *9*, 327–332.
69. Barra, D.; Calderoni, G.; Cinque, A.; De Vita, P.; Rosskopf, C.; Russo Ermolli, E. New data on the evolution of the Sele river coastal plain (Southern Italy) during the Holocene. *Il Quat.* **1998**, *11*, 287–299.
70. Amato, V.; Aucelli, P.; Ciampo, G.; Cinque, A.; Di Donato, V.; Pappone, G.; Petrosino, P.; Romano, P.; Rosskopf, C.; Russo Ermolli, E. Relative sea level changes and palaeogeographical evolution of the southern Sele Plain (Italy) during the Holocene. *Quatern. Intern.* **2013**, *288*, 112–128. [CrossRef]
71. Amorosi, A.; Pacifico, A.; Rossi, V.; Ruberti, D. Late Quaternary incision and deposition in an active volcanic setting: The Volturno valley fill, southern Italy. *Sedim. Geol.* **2012**, *282*, 307–320. [CrossRef]
72. Amorosi, A.; Molisso, F.; Pacifico, A.; Rossi, V.; Ruberti, D.; Sacchi, M.; Vigliotti, M. The Holocene evolution of the Volturno river coastal plain (Southern Italy). *J. Mediterr. Earth Sci.* **2013**, *11*, 7–11.
73. Santangelo, N.; Romano, P.; Ascione, A.; Russo Ermolli, E. Quaternary evolution of the Southern Apennines coastal plains: A review. *Geol. Carpath.* **2017**, *68*, 43–56. [CrossRef]
74. Bartole, R.; Savelli, D.; Tramontana, M.; Wezel, F.C. Structural and sedimentary features in the Tyrrhenian margin off Campania. *Mar. Geol.* **1984**, *55*, 163–180. [CrossRef]
75. Argnani, A.; Trincardi, F. Paola slope basin: Evidence of regional contraction on the Eastern Tyrrhenian margin. *Mem. Soc. Geol. Ital.* **1990**, *44*, 93–105.
76. Agate, M.; Catalano, R.; Infuso, S.; Lucido, M.; Mirabile, L.; Sulli, A. Structural evolution of the Northern Sicily continental margin during the Plio-Pleistocene. In *Geological Development of the Sicilian-Tunisian Platform*, 1st ed.; Max, M.D., Colantoni, P., Eds.; Unesco: Paris, France, 1993; Volume 58, pp. 25–30.
77. Hyppolite, J.C.; Angelier, J.; Barrier, M. Compressional and extensional tectonics in an arc system: Example of the Southern Apennines. *J. Struct. Geol.* **1995**, *17*, 1725–1740. [CrossRef]
78. Aiello, G.; Marsella, E.; Sacchi, M. Quaternary structural evolution of Terracina and Gaeta basins (Eastern Tyrrhenian margin, Italy). *Rend. Lincei* **2000**, *11*, 41–58. [CrossRef]
79. Caiazzo, C.; Ascione, A.; Cinque, A. Late Tertiary-Quaternary tectonics of the Southern Apennines (Italy): New evidences from the Tyrrhenian slope. *Tectonophysics* **2006**, *421*, 23–51. [CrossRef]
80. D'Argenio, B.; Pescatore, T.; Scandone, P. Schema geologico dell'Appennino meridionale. In *Atti del Convegno Moderne Vedute sulla Geologia Dell'appennino 1973*; Accademia Nazionale dei Lincei: Rome, Italy, 1973; Volume 183, pp. 49–72.

81. Bigi, G.; Bonardi, G.; Catalano, R.; Cosentino, D.; Lentini, F.; Parotto, M.; Sartori, R.; Scandone, P.; Turco, E. *Structural Model of Italy, 1:500.000*; Consiglio Nazionale delle Ricerche: Rome, Italy, 1992.
82. Aiello, G. Submarine Stratigraphy of the Eastern Bay of Naples: New Seismo-Stratigraphic Data and Implications for the Somma-Vesuvius and Campi Flegrei Volcanic Activity. *J. Mar. Sci. Eng.* **2022**, *10*, 1520. [CrossRef]
83. Aiello, G.; Sacchi, M. New morpho-bathymetric data on marine hazard in the offshore of Gulf of Naples (Southern Italy). *Nat. Hazards* **2022**, *111*, 2881–2908. [CrossRef]
84. Milia, A.; Torrente, M.M. Late Quaternary volcanism and transtensional tectonics in the Bay of Naples, Campanian continental margin, Italy. *Mineral. Petrol.* **2003**, *79*, 49–65. [CrossRef]
85. Sacchi, M.; Passaro, S.; Molisso, F.; Matano, F.; Steinmann, L.; Spiess, V.; Pepe, F.; Corradino, M.; Caccavale, M.; Tamburrino, S.; et al. The holocene marine record of unrest, volcanism, and hydrothermal activity of Campi Flegrei and Somma–Vesuvius. In *Vesuvius, Campi Flegrei, and Campanian Volcanism*, 1st ed.; De Vivo, B., Belkin, H.E., Rolandi, G., Eds.; Elsevier Science Publishers: Amsterdam, The Netherlands, 2020; pp. 435–469.
86. Sacchi, M.; Matano, F.; Molisso, F.; Passaro, S.; Caccavale, M.; Di Martino, G.; Guarino, A.; Innangi, S.; Tamburrino, S.; Tonielli, R.; et al. Geological framework of the Bagnoli–Coroglio coastal zone and continental shelf, Pozzuoli (Napoli) Bay. *Chem. Ecol.* **2020**, *36*, 529–549. [CrossRef]
87. Passaro, S.; Sacchi, M.; Tamburrino, S.; Ventura, G. Fluid Vents, Flank Instability, and Seafloor Processes along the Submarine Slopes of the Somma-Vesuvius Volcano, Eastern Tyrrhenian Margin. *Geosciences* **2018**, *8*, 60. [CrossRef]
88. Giaccio, B.; Hajdas, I.; Isaia, R.; Deino, A.; Nomade, S. High-precision $^{14}$C and $^{40}$Ar/$^{39}$Ar dating of the Campanian Ignimbrite (Y-5) reconciles the time-scales of climatic-cultural processes at 40 ka. *Sci. Rep.* **2017**, *7*, 45940. [CrossRef] [PubMed]
89. Romano, P.; Di Vito, M.A.; Giampaola, D.; Cinque, A.; Bartoli, C.; Boenzi, G.; Di Marco, M.; Giglio, M.; Iodice, S.; Liuzza, V.; et al. Intersection of exogenous, endogenous and anthropogenic factors in the Holocene landscape: A study of the Naples coastline during the last 6000 years. *Quat. Intern.* **2013**, *303*, 107–119. [CrossRef]
90. Vacchi, M.; Russo Ermolli, E.; Morhange, C.; Ruello, M.R.; Di Donato, V.; Di Vito, M.A.; Giampaola, D.; Carsana, V.; Liuzza, V.; Cinque, A.; et al. Millennial variability of rates of sea-level rise in the ancient harbour of Naples (Italy, western Mediterranean Sea). *Quat. Res.* **2020**, *93*, 284–298. [CrossRef]
91. Fedele, L.; Morra, V.; Perrotta, A.; Scarpati, C. *Carta Geologica Regionale alla Scala 1:10.000. Isole di Procida e Vivara (con Note Illustrative)*; Regione Campania, Settore Difesa del Suolo, Geotermia e Geotecnica: Napoli, Italy, 2012.
92. Sacchi, M.; Insinga, D.; Milia, A.; Molisso, F.; Raspini, A.; Torrente, M.M.; Conforti, A. Stratigraphic signature of the Vesuvius 79 AD event off the Sarno prodelta system, Naples Bay. *Mar. Geol.* **2005**, *222–223*, 443–469. [CrossRef]
93. Molisso, F.; Insinga, D.; Marzaioli, F.; Sacchi, M.; Lubritto, C. Radiocarbon dating versus volcanic event stratigraphy: Age modelling of Quaternary marine sequences in the coastal region of the Eastern Tyrrhenian Sea. *Nucl. Instrum. Methods Phys. Res.* **2010**, *268*, 1236–1240. [CrossRef]
94. Insinga, D.D.; Petrosino, P.; Alberico, I.; De Lange, G.J.; Lubritto, C.; Molisso, F.; Sacchi, M.; Sulpizio, R.; Wu, J.; Lirer, F. The Late Holocene tephra record of the central Mediterranean Sea: Mapping occurrences and new potential isochrons for the 4.4–2.0 ka time interval. *J. Quat. Sci.* **2020**, *35*, 213–231. [CrossRef]
95. Hsü, K.J.; Montadert, L.; Bernouilli, D.; Cita, M.B.; Erikson, A.; Garrison, R.G.; Kidd, R.B.; Mélières, F.; Müller, C.; Wright, R. History of the Mediterranean salinity crisis. In *Initial Reports of the Deep Sea Drilling Project 42A*; US Government Printing Office: Washington, DC, USA, 1978; pp. 1053–1078.
96. Bertoni, C.; Cartwright, J. 3D seismic analysis of slope-confined canyons from the Plio-Pleistocene of the Ebro Continental Margin (Western Mediterranean). *Basin Res.* **2005**, *17*, 43–62. [CrossRef]
97. Ridente, D.; Foglini, F.; Minisini, D.; Trincardi, F.; Verdicchio, G. Shelf-edge erosion, sediment failure and inception of Bari Canyon on the Southwestern Adriatic Margin (Central Mediterranean). *Mar. Geol.* **2007**, *246*, 193–207. [CrossRef]
98. Gamberi, F.; Della Valle, G.; Marani, M.; Mercorella, A.; Distefano, S.; Di Stefano, A. Tectonic controls on sedimentary system along the continental slope of the central and southeastern Tyrrhenian Sea. *Ital. J. Geosci.* **2019**, *138*, 317–332. [CrossRef]
99. Torrente, M.M.; Milia, A.; Bellucci, F.; Rolandi, G. Extensional tectonics in the Campania Volcanic Zone (eastern Tyrrhenian Sea, Italy): New insights into the relationship between faulting and ignimbrite eruptions. *Ital. J. Geosci.* **2010**, *129*, 297–315.
100. Pérès, J.M.; Picard, J. Nouveau manuel de bionomie benthique. *Recl. Des Trav. De La Stn. Mar. D'endoume* **1964**, *31*, 5–137.
101. Brandano, M.; Civitelli, G. Non-seagrass meadow sedimentary facies of the Pontinian Islands, Tyrrhenian Sea: A modern example of mixed carbonate–siliciclastic sedimentation. *Sedim. Geol.* **2007**, *201*, 286–301. [CrossRef]
102. Aiello, G.; Caccavale, M. From Siliciclastic to Bioclastic Deposits in the Gulf of Naples: New Highlights from Offshore Ischia and Procida-Pozzuoli Based on Sedimentological and Seismo-Stratigraphic Data. *Quaternary* **2021**, *4*, 44. [CrossRef]
103. Steinmann, L.; Spiess, V.; Sacchi, M. The Campi Flegrei caldera (Italy): Formation and evolution in interplay with sea-level variations since the Campanian Ignimbrite eruption at 39 ka. *J. Volcanol. Geotherm. Res.* **2016**, *327*, 361–374. [CrossRef]